

Scaling the ice strength

What are the limitations of using local ice strength measurements from the Borehole Jack and brine based estimations to determine a site-specific $C_{\rm R}$ coefficient according to the ISO 19906 guideline?

M. Wilmink

Student number: 4960785

Thesis duration: January 1, 2025 – July 8, 2025

Thesis committee: Dr. ir. H. Hendrikse, TU Delft, supervisor

Prof. Dr. K. V. Høyland, NTNU, supervisor

Dr. ir. P. van der Male, TU Delft Ir. J. S. Hoving, TU Delft

Universities: TU Delft & NTNU

Cover: Hjellbotn, Norway during the case study in January 2025.







Preface

The completion of this thesis marks not only the end of my Master's degree, but also the conclusion of seven years of studying. It began in Delft, as a wide-eyed student who thought he knew something about math and physics and liked boats, only to discover he knew very little about math, physics and boats. Over the years, both TU Delft and NTNU have taught me to question the world around me. I can't walk past a crane without visualizing the forces running through every beam and joint—and wondering whether the entire structure could be done smarter, lighter, or more efficiently. Lighter is not always the answer.

I am deeply grateful to Knut Vilhelm Høyland for giving me the opportunity to work on the ice, handson, outdoors and exposed to the elements. This project allowed me to test something real, under real conditions. Who knows what role these results might play in the next 50 years. Perhaps, one day we'll have wind turbines in retreating ice packs while seeing the ice grow back. Time will tell.

Working with people from different backgrounds and nationalities has taught me a great deal—about communication, collaboration, and the value of diverse perspectives. Planning and executing fieldwork taught me the importance of preparation and adaptability. I want to sincerely thank Knut for always being available, whether in his office or online. His practical guidance during fieldwork was invaluable, and his calm support throughout the process helped me move forward with clarity.

I would also like to thank Hayo Hendrikse for his thorough feedback and constructive criticism. His ability to view the work from a different angle and always justify each comment with insight and actionable suggestions which helped me to get further in this thesis instead of staying stuck.

Finally, to my girlfriend: thank you for the daily pep talks that helped me stay on track. And to my friends: thank you for the laughs and cooking dinner when the workload was piling up. You all made this journey not only possible, but a lot more fun along the way.

Delft, July 2025
Max Wilmink

Abstract

As offshore wind energy is expanding into seasonally ice-covered regions, accurate estimation of sea ice strength becomes critical for safe and cost-effective design. ISO 19906 provides an empirical method to estimate the global ice force based on the width of the structure, thickness of the ice, and an ice strength coefficient, $C_{\rm R}$. It suggests predefined reference values for this coefficient depending on the region of interest. However, if the wind farm will be located outside one of these predefined reference regions, the ISO standard gives limited guidance on how to adjust the ice strength coefficient to the local ice conditions. This study investigates the method proposed in ISO 19906 to estimate a site-specific ice strength coefficient, $C_{\rm R,s}$. The method uses the ratio of the ice strength index obtained from strength measurements at a reference site and a new site.

In this study, two sites were selected to determine this strength index ratio. Hjellbotn, a temperate brackish ice zone near Trondheim, was selected as a potential offshore wind site and falls outside ISO's predefined $C_{\rm R}$ regions. Svea, in the Svalbard archipelago, was used as a proxy for the Arctic region for which the ice strength coefficient has been determined by ISO. The ice strength index at both locations was estimated using two ISO-recommended approaches: a direct mechanical measurement with the BHJ and an indirect estimate based on brine volume derived from temperature and salinity. ISO 19906 provides a predefined ice strength index for the Arctic region when using the brine volume method. However, the standard does not offer a similar reference value for measurements taken with the BHJ. BHJ tests from Svea were used to represent the Arctic BHJ reference. The same test procedure was used at Hjellbotn for comparison. The BHJ strength ratio suggested lowering the ice strength coefficient for Hiellbotn. Brine-based strength ratios used either the ISO Arctic reference or Svea data. The ISO-based approach also indicated a lower strength coefficient for Hjellbotn, as expected for more temperate ice. Using Svea as the proxy for the Arctic gave a higher strength coefficient for Hjellbotn, which was unexpected. It showed that the choice of method and reference value affects the outcome of the strength estimation. This difference indicated a limitation of the brine volume strength method when trying to scale the ice strength coefficient from the Arctic to warm ice conditions. For warm ice, small temperature changes caused large strength variations, which showed the brine-based method's high sensitivity.

The results of this work suggest that while the ISO framework provides a basis for estimating an ice strength coefficient for a new area, careful interpretation is required when scaling the ice strength from an Arctic region to temperate and marginal ice zones. The brine volume method is sensitive to measurement uncertainty at high ice temperatures and may not always reflect the full mechanical strength of the ice.

Contents

Pr	eface	İ
Lis	st of Tables	iv
Lis	st of Figures	vi
No	omenclature	vii
1	Introduction 1.1 Background and Motivation	1 1 2 2
2	Theoretical Background 2.1 Ice Strength for Offshore Wind 2.2 Sea Ice Formation and Mechanical Properties 2.3 Measurement Methods 2.4 ISO 19906 Global Ice Pressure and Strength Coefficient CR	4 4 5 6
3	Method3.1 Approach3.2 Study Locations3.3 The Borehole Jack3.4 Ice Property Measurements	18 19 21 26
4	Results 4.1 Borehole Jack Calibration	30 30 30 37 41
5	Discussion 5.1 Reduction Factor: Svea vs. Hjellbotn 5.2 Influence of Ice Conditions on Measured Strength 5.3 Temperature Sensitivity in the Brine Volume Estimation 5.4 Validity of the predefined Arctic ISO Reference value 5.5 Limitations	45 46 48 49 49
6	Conclusion	51
7	Recommendations	53
Α	Boreholejack Results A.1 Hjellbotn	56 56

List of Tables

2.1	Suggested default $C_{R,0}$ values based on Freezing Degree Days, including example locations (ISO19906, 2019)	9
2.2	Ice-strength coefficient ${\it C}$ as a function of brine volume $v_{\rm b}$ (from ISO 19906, Table A.8-5).	10
4.1	Correction factor c with standard deviation from calibration tests	30
4.2	Maximum measured BHJ pressure and failure observation for the two tests performed in each hole at Hjellbotn. A calibration factor of 2.13 was used to obtain the BHJ strength.	33
4.3	Measured salinity values for each layer in ppt from two cores retrieved at Hjellbotn	35
4.4	Ice density for each layer at Hjellbotn, retrieved from samples of Hole 3 and Hole 5	36
4.5	Maximum measured BHJ pressure for the two tests performed in each hole at Svea.	-
	Tests were carried out between 26 and 28 March 2025	38
4.6	Calculated brine volume using the ISO A.6-6 and UNESCO method over different tem-	
	perature values with a fixed salinity of 0.16 ppt	41
4.7	Brine volume calculated using the ISO A.6-6 and UNESCO method over different tem-	
	perature values with a fixed salinity of 5.73 ppt	41
4.8	Overview of ice strength index values from BHJ tests at Hjellbotn (specific area of inter-	
	est) and Svea (reference area)	42
	Summary of ice strength index values $\sigma_{{\sf Bri},x}$, based on the brine volume method	42
	Sensitivity of $\sigma_{\rm Bri}$ to temperature changes for warm ice at a fixed salinity of 0.16 ppt	43
	Sensitivity of $\sigma_{\rm Bri}$ to temperature change in cold ice at a fixed salinity of 5.73 ppt	43
4.12	Reduction factors based on the brine volume method. Each factor is defined as $R_{x,y} =$	
	$(\sigma_{\text{Bri},x,s}/\sigma_{\text{Bri},y,0})$, where x denotes the method used for the specific area of interest and y	
	the method or reference value used for the reference area	44
4.13	Change in $R_{is,A}$ and corresponding scaled ice strength coefficient $C_{R,s}$ with temperature	
	at Hjellbotn. Values are calculated using the ISO Arctic reference strength $\sigma_{\text{Bri},A,0} = 2.86$ MPa and a fixed salinity of 0.16 ppt.	44
	ίνιι α απά α πλεά θαιπτίες οι ό. το ρρε.	
5.1	Comparison of strength estimates and reduction factors using BHJ and brine methods.	46

List of Figures

2.1 2.2	Four common stress-displacement response types observed during BHJ tests. Adapted from Sinha et al. (2012)	6 8
2.3 2.4	Interpolated ice strength coefficient C_{Bri} vs brine volume v_{b} , based on ISO 19906 data. Vertical decision flowchart for scaling the ice strength coefficient C_{R} using ISO 19906. If the brine volume method is used, $\sigma_{\text{Bri},0}$ can be either taken from ISO or calculated from a reference profile	11
3.1	An overview grid of the location of the Hjellbotn area. Retrieved from: Google Earth, 2023 Landsat/CopernicusDataSIO, NOAA, U.S.Navy, NGA, GEBCO IBCAO a : A view of Scandinavia and a part of Europe showing the location of the Fjord with a blue marker. b : A zoomed in view of part of Norway, showing the location of Hjellbotn in the Trondheim-Fjord, c : A view of the northern part of the Trondheimfjord, with red circles highlighting the small canals that connect Hjellbotn to the larger Fjord. d : A 3D view of Hjellbotn. From (Wilmink, 2024).	19
3.2	Study area overview maps	21
3.3	Overview of the Borehole Jack design and mechanics. (a) shows a technical drawing of the jack in an ice sheet, (b) shows the exposed gear system at the top of the unit	22
3.4	Photograph with detailed views of the BHJ. a : Load cells and threaded rod. b : Gearing system. c : Piston extended. d : Piston retracted	23
3.5	Photograph of the BHJ including field laptop, transportation case and logger box in field testing mode	24
3.6	Schematic overview of the BHJ calibration setup. (a) shows the unloaded position, and (b) shows the configuration under full extension.	25
3.7	Photographs of the BHJ calibration rig at NTNU. (a) shows the back view where the BHJ is inserted into the rig, and (b) presents a zoomed-in side view with a clear view of the	
3.8	load cell setup	26 27
3.9	Examples of equipment used for ice property measurements and ice strength measurements.	28
3.10	Preparation and Hydrostatic weighing setup in the NTNU cold laboratory	29
4.1	Daily mean air temperature at Steinkjer (weather station 11 km from the Hjellbotn testsite, 12.1 m above sea level) and Akseløya (Weather station 40 km from the Svea testsite, 15 m above sea level). The dashed green line indicates the first field visit after a storm at Hjellbotn (21 January 2025). The red dashed line marks the day when the measurements at Hjellbotn were carried out (29 January 2025). The grey zone marks the period when the measurements at Svea were carried out (26-28 March 2025)	31
4.2	Photographs of the shoreline conditions at Hjellbotn during the initial site visit on 21st of January 2025.	32
4.3	Photographs of the ice layers at Hjellbotn retrieved on 29 January 2025. Distinct stratification is visible, with a solid ice layer at the bottom and a more porous layer at the top.	32
4.4	Borehole Jack pressure over time curves from hole 2 and 3 performed at Hjellbotn. Visual inspection confirmed no spalling occurred in either tests.	33
4.5	Examples of spalling after BHJ measurements in Hiellboth in holes 1 and 4	34

List of Figures vi

4.6	Borehole Jack pressure-time curves from Hole 1 and Hole 4 at Hjellbotn, where spalling was observed. Visual inspection confirmed spalling in both tests, upward and downward	
	in Hole 1, and upward in Hole 4	34
4.7	Average ice temperatures at Hjellbotn in February 2025, recorded by thermistor sensors	
	12, 13, and 14 in the 12-14 cm thick ice sheet	35
4.8	Estimated probability of bending versus crushing failure as a function of ice thickness.	
	(Hendrikse, 2024)	37
4.9	Borehole Jack pressure over time curves from Hole 5 and Hole 6 at Svea	38
4.10	Vertical ice temperature profile from Svea. Values represent the average of 10 layers	
	over the normalized depth. Graph obtained from course report: (UNIS, 2025)	39
4.11	Average vertical salinity profile at Svea. A C-shaped curve is visible, with peak values	
	near the ice surface and bottom. Graph obtained from course report: (UNIS, 2025)	39
4.12	Vertical density profile from a representative ice core at Svea. A rapid increase is seen	40
	in the upper part of the ice. Graph obtained from course report: (UNIS, 2025)	40
5.1	Maximum BHJ pressure measured at a depth interval of 10 cm in the 60 cm thick ice	
0.1	sheet at Svea. The plot shows how strength varies with depth, showing a peak in the	
	middle layers with the top and bottom layers significantly weaker.	47
	3, 1, 1, 1, 1, 1, 1, 1, 1, 1, 1, 1, 1, 1,	
A.1	Pressure vs Time plots for selected Hjellbotn BHJ tests, showing peak pressure and	
	observed failure mode	56
	Pressure vs Time plots for Hole 1 and Hole 2 tests at Hjellbotn	56
	Pressure vs Time plots for Hole 3 and Hole 4 tests at Hjellbotn	57
A.4	Pressure vs Time plots for Hole 5 and Hole 6 tests at Hjellbotn	57
A.5	Pressure vs Time plots for Hole 1 and Hole 2 at Svea	58
A.6	Pressure vs Time plots for Hole 3 and Hole 4 at Svea	59
A.7	Pressure vs Time plots for Hole 5 and Hole 6 at Svea	59
	Pressure vs Time plots for Hole 7 and Hole 8 at Svea	60
A.9	Pressure vs Time plots for Hole 9 at Svea	60

Nomenclature

Regular Symbols

Symbol	Description	Unit
C_{Bri}	Strength coefficient from brine volume	MPa
$C_{Bri,i}$	Strength coefficient for layer <i>i</i> from brine volume	MPa
C_{R}	Ice strength coefficient	MPa
$C_{R,0}$	Ice strength coefficient for reference area	MPa
$C_{R,s}$	Ice strength coefficient for specific area of interest	MPa
d	Diameter of the pile	m
f_{AR}	Empirical aspect ratio shape correction factor	-
F_{G}	Global ice action normal to structure surface	N
h	Ice thickness	m
h_1	Reference unit ice thickness	m
m	Empirical coefficient in global ice strength relationship	-
m_{air}	Mass of ice block in air	g
$m_{\sf par}$	Mass of ice block submerged in paraffin	g
n	Empirical coefficient in global ice strength relationship	-
n	Thickness exponent or number of layers	-
p_{G}	Global average pressure	MPa
R	Reduction factor	_
R_{BHJ}	Reduction factor based on BHJ strength	_
R_{Bri}	Reduction factor based on brine-volume	_
$R_{Bri,u,A}$	Reduction factor based on brine-volume from UNESCO and Arctic reference	-
$R_{Bri,u,f}$	Reduction factor based on brine-volume from UNESCO and Frankenstein	-
S	Bulk salinity of sea ice	ppt
S_{b}	Brine salinity	ppt
$S_{i,s}$	Ice salinity in specific area of interest	ppt
$S_{i,0}$	Ice salinity in reference area	ppt
T	Ice temperature	°C
$T_{air,i}$	Daily average air temperature	$^{\circ}C$
T_{f}	Freezing point of seawater or brine	$^{\circ}C$
$T_{\sf measured}$	Measured ice temperature	$^{\circ}C$
$T_{i,s}$	Ice temperature of layer in specific area of interest	$^{\circ}C$
$T_{i,0}$	Ice temperature of layer in reference area	$^{\circ}C$
v_{b}	Brine volume fraction	-
$v_{b,is}$	Brine volume based on ISO method	-
$v_{\sf b,is,s}$	Brine volume based on ISO method in specific area of interest	-
$v_{\sf b,is,0}$	Brine volume based on ISO method in reference area	_
$v_{\sf b,u,s}$	Brine volume based on UNESCO method for specific area of interest	_
$v_{b,f,0}$	Brine volume based on Frankenstein method in reference area	-
$v_{b,corr}$	Brine volume correction factor	-
w	Structure width	m

List of Figures viii

Greek Symbols

Symbol	Description	Unit
ρ_{ice}	Density of ice	kg/m ³
$ ho_{\sf par}$	Density of paraffin	kg/m³
σ	Measured or inferred ice strength index	MPa
σ_{Bri}	Measured or inferred brine-volume-based strength index	MPa
$\sigma_{\sf Bri,s}$	Measured brine-based strength index for specific area of interest	MPa
$\sigma_{Bri,0}$	Measured or inferred brine-based strength index in reference area	MPa
σ Bri,A,0	Inferred brine-based strength index for Arctic reference region (ISO)	MPa
$\sigma_{Bri,f,0}$	Measured brine-based strength index based on Frankenstein method	MPa
$\sigma_{Bri,T,0}$	Inferred brine-based strength index for temperate reference regions (ISO)	MPa
$\sigma_{\sf Bri,u,s}$	Measured Brine-based strength index for specific area of interest (UNESCO method)	MPa
$\sigma_{BHJ.s}$	Measured BHJ-derived strength index for specific area of interest	MPa
$\sigma_{BHJ,0}$	Measured BHJ-derived strength index for reference area	MPa
σ_0	Measured or inferred strength index for the reference area	MPa
$\sigma_{ t s}$	Measured Strength index for specific area of interest	MPa

1

Introduction

As global energy demand increases and the shift toward renewable energy accelerates, offshore wind is expanding into higher latitudes. In these colder regions, seasonal sea ice becomes a critical design factor for offshore structures. Understanding how sea ice interacts with offshore foundations is essential to ensure safe and reliable installations. The strength of the ice has a significant influence on the maximum force that structures must be able to resist, which makes accurate estimation of ice strength essential to avoid both structural failure and overly conservative designs (Shi, 2020).

Driven by the European Green Deal, the European Union aims to expand its offshore wind capacity to 60 GW by 2030 and 300 GW by 2050 (Parliament, 2020). This expansion pushes development into northern waters, where sea ice is present in the winter season. In parallel, China has set even higher targets and aims for 800 GW of offshore wind by 2030 and 3000 GW by 2060 (Liu et al., 2023). Construction has already started in the Bohai Sea, a coastal region regularly affected by seasonal ice (Li et al., 2024).

This expansion into ice-affected areas shows that there is a need for a better local understanding of ice actions. In particular, the compressive strength component of the ice forces and ice strength should be studied further. Reliable strength estimates are important to optimize structural design and to ensure the long-term durability of offshore wind farms in cold environments. Despite the importance, there are large uncertainties in estimating ice strength in these new regions. Existing design standards, like ISO 19906, are mainly based on Arctic multi-year ice and old data from the Baltic. The applicability of Arctic-based ice strength parameters to warm, seasonal, first-year ice environments remains poorly validated. Without site-specific adaptations, designs may become unsafe, unreliable or inefficient.

1.1. Background and Motivation

The design of offshore structures in ice-covered waters is complicated by the significant and uncertain forces generated by sea ice. Loads must be predicted accurately to ensure safety while avoiding overly conservative designs. Conservatism increases material use, costs, and environmental footprint. The need for improved ice load estimation grows as offshore wind activities expand into seasonally ice-covered seas. The international design standard, ISO19906, used for offshore structures in ice-covered waters, was originally developed with petroleum structures in mind. First published in 2010 and updated in 2019, ISO 19906 provides semi-empirical methods for estimating global ice forces (ISO19906, 2019). It introduces the crushing strength coefficient, $C_{\rm R}$, which represents the effective strength of sea ice. Although $C_{\rm R}$ accounts for variability in ice properties, strain rate, and environmental exposure, the contribution of each factor remains unknown.

The design challenges for offshore wind turbines differ from those faced by traditional petroleum platforms. In the Arctic, structures are exposed to thick, heavy ice, including ridges driven by strong forces, with a lot of exposure. On the other hand, for more temperate regions like the Baltic Sea, the design ice is much thinner, between 0.2 and 1.2 m (Høyland et al., 2023). Wind turbine foundations are slender and flexible, making them considerably more sensitive to dynamic ice-structure interactions (Hendrikse, 2017). In contrast, oil and gas platforms are typically large, stiff, and respond almost quasi-statically when impacted by ice. Because of these differences, it is uncertain whether knowledge gained from lighthouses and offshore platforms can be applied to wind turbine structures (Høyland et al., 2023).

Nominal $C_{\rm R}$ values are based on limited field datasets. ISO recommends a value of 2.8 MPa for Arctic conditions, derived from Beaufort Sea measurements, and 1.8 MPa for temperate regions, based on data from Norströmsgrund (Hendrikse & Owen, 2023). An intermediate value of 2.4 MPa is suggested for sub-Arctic conditions, interpolated without direct measurement-based support. However, when one is interested in a value of $C_{\rm R}$ for a region not mentioned in ISO, guidance appears to be limited. ISO 19906 provides a framework to scale the ice strength based on in-situ tests and ice strength obtained from brine volume and temperature. It recommends performing strength measurements in the area of interest and a reference area for which a $C_{\rm R}$ has already been determined (Arctic or Temperate). By obtaining the difference in ice strength between the measured areas, a locally adjusted $C_{\rm R,s}$ can be found. ISO proposes the use of a borehole jack (BHJ) to directly obtain a compressive strength index. An indirect approach by using the brine volume obtained from salinity and temperature measurements is also proposed. However, it does not specify how the input parameters should be selected or how the scaling should be validated in practice. This leaves application of the scaling equation open to interpretation. Using nominal $C_{\rm R}$ values without local adaptation may lead to unsafe or uneconomical designs.

Another challenge lies in measuring the ice strength. Several in-situ strength methods are proposed in ISO, including uniaxial compression, point-load, and BHJ tests (ISO19906, 2019). The BHJ is practical for field campaigns and provides direct strength measurements. However, no standard BHJ design exists. Devices differ in loading method (mechanical or hydraulic), geometry, and contact area. These differences complicate comparisons across studies. Because of these uncertainties, there is a gap in the literature on how to consistently determine site-specific ice strength parameters from field data. Particularly for offshore wind projects, which involve many support structures, small improvements in strength estimates can yield large cost and environmental benefits.

1.2. Research Objective

While the proposed scaling method is relatively straightforward in theory, its practical application is complicated by a lack of guidance on how to select appropriate strength indices and reference values. For the brine volume method, ISO suggests a reference value for the Arctic and Temperate region. A strength index for the specific area of interest needs to be measured to obtain a local $C_{\rm R,s}$. On the other hand, the standard does not provide an equivalent reference strength index for the BHJ method. This introduces significant uncertainty when applying the scaling method in environments that differ from those used to develop the original ISO coefficients.

The ISO approach assumes that different strength estimation methods yield a consistent reduction or increase in strength when compared with each other. This study investigates the limitations of using the ISO 19906 scaling method to derive reliable site-specific $C_{\rm R,s}$ values using in-situ BHJ measurements and ice property data. This study conducted a case study in two different environments, Hjellbotn in the mainland of Norway served as the area of interest and Svea in the Norwegian archipelago of Svalbard served as the reference area. The work studies whether mechanical and property based strength estimates result in consistent scaling outcomes. It also explains how how deviations between test methods can affect design outcomes for offshore wind structures.

1.3. Structure of the Thesis

This study is organized to first build a theoretical foundation in sea ice mechanics and then present the method, experimental work and findings. Chapter 2 introduces the theoretical background on sea ice mechanics, ice strength parameters, and the definition and application of the $C_{\rm R}$ coefficient. It also reviews the BHJ testing method and discusses how its measurements can be interpreted. Chapter 3 describes the selected field sites, outlines the fieldwork procedures, explains the BHJ calibration process, and presents the data processing methods. Chapter 4 presents the results from the field and laboratory campaigns, including BHJ strength measurements, ice salinity and temperature profiles, and the strength indices derived from these properties. Chapter 5 discusses the results in relation to

existing standards, previous studies, and the challenges of adapting ISO 19906 to local conditions. Finally, Chapter 6 summarizes the main findings of this study and provides recommendations for future research directions.

Theoretical Background

This chapter introduces the theoretical background necessary to understand sea ice actions on structures and what influences how the sea ice strength is scaled. It first explains how ice fails when it interacts with offshore wind turbines and which factors control its mechanical behavior. The chapter explains how the international design standard (ISO) uses the $C_{\rm R}$ coefficient to include the ice strength in the ice action equations. It describes the assumptions behind this coefficient, the parameters used to determine the strength, and how it was originally obtained. The Borehole Jack method for in-situ strength measurements is introduced as a tool for field studies. Finally, previous studies that investigated site-specific scaling of ice strength are reviewed. Their findings are discussed to show the challenges and uncertainties in adapting the ISO 19906 method to local ice conditions.

2.1. Ice Strength for Offshore Wind

The expansion of offshore wind energy into ice-covered seas, such as the Baltic and other temperate regions, introduces significant design challenges. In these areas, wind turbine foundations may be subjected to considerable loads from level sea ice. The LOLEIF and STRICE field studies at Norströmsgrund suggested that crushing is the main failure mode at vertical-sided structures (Schwarz & Jochmann, 2001). Inclined or conical foundations often reduce horizontal loads by causing the ice to fail in bending. However, they also increase wave loads and construction costs because of their larger diameter at the waterline. For this reason, this study focuses on crushing at the waterline. In this work, *ice strength* refers mainly to the compressive strength of level sea ice. During crushing, ice fails in compression after contact with the structure. This process can produce high local pressures and global loads. Monopile foundations differ significantly from traditional oil and gas structures. Wind turbines are often more compliant than other Arctic offshore structures. This makes them more prone to dynamic amplification and resonant responses during ice-structure interaction (Kamesaki, 1996).

Current design standards rely on empirical data obtained from earlier full-scale campaigns. The proposed ice action equations in the ISO19906 standard are based on data from the Molikpaq platform in the Beaufort Sea around 1980 and the Norströmsgrund Lighthouse in the Gulf of Bothnia around 2000. Even these structures experienced dynamic amplification while being considerably stiffer than wind turbines. The ice conditions at those sites were more severe than those in more temperate regions. As such, the direct application of these empirical methods introduces uncertainty for wind turbine design in more temperate regions.

Ice thickness, drift speed, ice strength, ice-structure friction, and the structural geometry of the structure all influence the magnitude of the ice actions on the monopiles. Ice-induced vibrations occur because of the dynamic interactions between structures and crushing ice. Different types of ice-induced vibrations can occur, depending on the ice drift speed. These include intermittent crushing, frequency lock-in, and continuous brittle crushing. Intermittent crushing and a newly observed type called multi-modal vibration can cause the highest bending forces and fatigue stresses in wind turbine structures (Hammer, 2024). These types of vibrations are strongly affected by the flexibility and natural frequencies of the

turbine. They mainly occur at low ice drift speeds and are difficult to design for because the dynamic loads can become much larger than the average force.

Comprehensive full-scale data for offshore wind turbines in ice infested areas is limited. As a result, further research is needed to improve understanding of ice loads on these structures (Høyland et al., 2023).

2.2. Sea Ice Formation and Mechanical Properties

Sea ice forms when the surface of seawater cools below its freezing point. When the temperature drops below approximately -1.9°C, the growth of frazil crystals starts. These are small, plate-like ice particles that accumulate at the surface. In areas with wave action, these crystals form a granular ice layer. Under calm conditions, columnar ice will develop with vertically aligned grains (Timco & Weeks, 2010). During freezing, not all the salt is expelled. Brine inclusions remain trapped between the growing ice crystals, leading to a porous structure composed of solid ice, liquid brine, and gas pockets (Goldstein & Osipenko, 2015). Over time, as the ice thickens and cools further, brine drains out of the ice which reduces the brine volume and increases the effective strength of the ice layer.

Granular ice tends to behave more isotropic due to the random crystal orientation. On the other hand, columnar ice shows anisotropic behavior, with mechanical properties depending on the loading direction relative to the grain alignment (Timco & Weeks, 2010).

2.2.1. Key Parameters Affecting Ice Strength

Sea ice is a complex material made up of solid ice crystals, liquid brine, and gas bubbles. Together, these components form the ice matrix. The ice crystals create the solid framework, while brine pockets and gas inclusions weaken the structure by interrupting stress paths (Weeks, 2010). Understanding how the properties of this matrix influence the compressive strength is important for interpreting field measurements and for designing safe offshore structures.

Several key parameters control the mechanical behavior of sea ice:

- **Temperature:** Temperature has a direct and strong influence on ice strength. As the temperature drops, more brine solidifies, stiffening the ice matrix and increasing its resistance to deformation (Timco & Weeks, 2010). Colder ice can also sustain higher strain rates before brittle fracture occurs. This dual effect makes temperature one of the most important factors in ice strength determination (Høyland, 2024).
- Salinity and Brine Volume: Salinity defines the amount of liquid brine trapped in the ice. Higher salinity results in higher brine volumes, which reduce the effective load-bearing area and thus lower strength (Timco & Weeks, 2010). Brine volume is calculated from salinity and temperature measurements. This will be further explained in Section 2.4.1.
- Porosity and Gas Content: Besides brine, gas bubbles contribute to the total porosity of sea ice. Increased porosity disrupts the stress-carrying network within the ice, further weakening it (Weeks, 2010). A high gas content is often found in ice formed through snow-ice processes, where seawater floods a snow layer and later freezes, trapping the air in the ice.
- **Grain Size and Microstructure:** The size, shape, and orientation of ice grains affect strength. Large grains make ice more prone to crack propagation along grain boundaries, reducing compressive strength (Weeks, 2010). Columnar ice, with grains aligned vertically, tends to be stronger than granular or layered structures (Høyland, 2024).
- Strain Rate: Ice is sensitive to the rate at which it is loaded. At low strain rates, ice deforms plastically, while at high strain rates it fractures in a brittle manner (Høyland, 2024). Laboratory studies show that strength increases with strain rate up to a critical point, after which it decreases again due to crack initiation and growth.
- Confinement Effects: Increased confinement results in a higher pressure from surrounding ice, which can also increase the apparent strength by preventing crack growth (Jones, 1982). When the surrounding ice restricts lateral expansion during compression, it suppresses the formation and propagation of tensile cracks. This allows the ice to withstand higher axial loads.

These parameters act together, not separately. For example, temperature affects both brine volume and strain-rate sensitivity. This makes it difficult to predict the sea ice strength based only on simple environmental measurements.

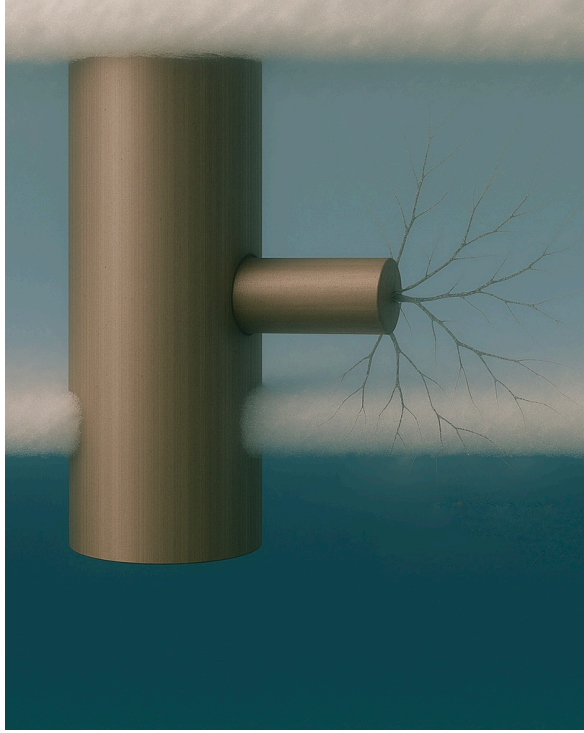
2.3. Measurement Methods

An accurate value for the compressive strength is essential for proper design. Several methods to measure the ice strength exist. Lab-scale measurements are influenced by natural ice variability and confinement scale effects. Larger ice volumes contain more flaws and the surrounding ice constrains the failure zone, resulting in lower apparent strength. Dempsey et al. (1999) demonstrated that tensile strength decreases with increasing sample size due to these effects. The same holds for compressive strength (Masterson & Graham, 1995). The LOLEIF campaign also indicated that field-measured ice loads on structures were significantly lower than those predicted using laboratory strength values (Schwarz & Weeks, 1977). In-situ methods are therefore preferred for realistic strength measurements.

Among the available field methods, the BHJ is one of the most widely used tools for measuring the in-situ confined compressive strength. It makes strength measurements possible directly within the ice. This is done without removing the sample or disturbing the internal structure. The BHJ test creates a radial stress field by expanding a piston inside a pre-drilled borehole while recording the applied load. The recording measures how much force is needed to press into the ice. A photograph of the BHJ is shown in Figure 2.1a. An illustration of the BHJ inserted in the ice sheet with the piston extended is shown in Figure 2.1b.



(a) Photograph of the Borehole Jack used for in-situ sea ice strength testing. The steel cylinder houses a horizontally oriented piston that can be extended to apply a force against the ice borehole wall. Photo taken at the NTNU, Trondheim.



(b) A zoomed-in, cross-sectional visual representation of the BHJ piston inserted in an ice sheet. The expansion of the piston into the ice can result in cracks that propagate into the ice. This illustration was generated to show the BHJ loading mechanism.

Figure 2.1: The Borehole Jack and a visual representation of the jack inserted in the ice.

Because of its portability and simplicity, the BHJ is especially useful for remote or temporary field campaigns. It allows for vertical profiling of strength by using the adjustable height plate. This enables the BHJ to detect local strength variations in the ice profile. For these reasons, BHJ measurements form the basis of strength analysis in this study. The historical development and design of the BHJ system are described in the next section.

2.3.1. Borehole Jack Method and Development

In-situ strength testing methods emerged in the early 1970s, as offshore development advanced into Arctic regions. Existing laboratory tests could not capture strength variation with depth or under realistic environmental conditions.

In 1971, Kivisild proposed adapting a geotechnical pressure-meter for use in sea ice. While the original tool was not strong enough for ice applications, the idea led to the first operational BHJ, built in 1974 by Masterson and Graham (1995). Their design used a single hydraulic piston to press against the borehole wall. It was compact and allowed vertical profiling of ice strength. The National Research Council of Canada improved this design in the 1980s by introducing the NRC-BHI system (Sinha, 2011). This version featured two opposing pistons for symmetrical loading and better repeatability. It also allowed controlled strain rate testing and was used to study both first-year and multi-year ice. Sinha later evaluated the BHJ for engineering design and mentioned the need for consistent procedures. It was noted that test results were sensitive to temperature, loading rate, and microstructure of the ice (Sinha, 1987).

A more recent version was developed for the Norwegian University of Science and Technology (NTNU) at M-Tech, Trondheim. This jack uses a mechanical system to push a piston outward by rotating a threaded rod with a cordless drill. Load sensors record internal forces, which are converted to radial pressure using a calibration factor. The version used in this study includes a dedicated calibration rig for improved accuracy. The rig is described in detail in Section 3.3.2. The BHJ method is now recognized as a valid in-situ strength measurement (ISO19906, 2019). These measurements, when combined with salinity, temperature, and structure data, provide a basis for evaluating local ice strength conditions. However, no standardized design exists for the Borehole Jack. As a result, data from different studies may not be directly comparable. For this reason, BHJ measurements are best interpreted as index values rather than absolute strength measurements.

2.3.2. Interpretation of BHJ Results

During a BHJ test, the piston expands laterally against the borehole wall, and the internal load is recorded over time. Since the BHJ used in this study operates at a constant displacement rate, the force-time and force-displacement plots are equivalent. Maintaining a constant indentation speed is crucial, as the mechanical response of ice is strain-rate dependent. The strength obtained from the BHJ test is adjusted using a calibration factor obtained from laboratory testing, as described in Section 3.3.2. The resulting effective radial pressure is taken as the compressive strength of the ice. Sinha et al. (2012) classified four typical response types observed in BHJ tests based on the shape of the stress-displacement curve:

- Flow Stress: The stress increases continuously with displacement without a clear peak. This mode is common in warm, young, or deteriorating ice. In these cases, strength can be described at a defined displacement such as 3 or 5 mm.
- **Asymptotic Strength**: The stress increases to a plateau and remains stable with further displacement. This is often observed in soft or decaying ice where the system cannot apply higher loads.
- Upper Yield: A peak stress is reached and followed by a drop, sometimes followed by a second rise. This behavior corresponds to ductile failure with micro-cracks and time-dependent deformation.
- **Premature Failure**: A sharp peak is followed by a sudden stress drop, typical of brittle failure. Multiple peaks may occur as new fractures develop with further displacement.

These four types are illustrated in Figure 2.2. In the current study, the maximum value from each test is used regardless of failure type. This approach is used because the maximum value is expected to best represent the crushing strength of the ice.

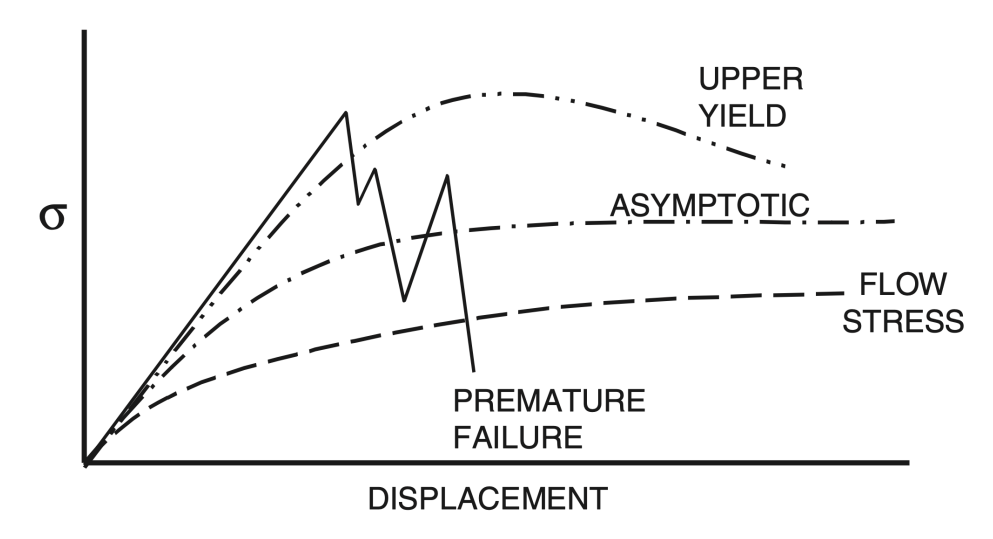


Figure 2.2: Four common stress-displacement response types observed during BHJ tests. Adapted from Sinha et al. (2012).

2.4. ISO 19906 Global Ice Pressure and Strength Coefficient $C_{\rm R}$

ISO 19906 provides an empirical formula to calculate the global ice action on a vertical structure due to crushing of level ice. The global force $F_{\rm G}$ in Equation (2.1) is expressed in terms of a global pressure $p_{\rm G}$ acting over the contact area $w \times h$, where w is the structure width and h the ice thickness.

$$F_{\mathsf{G}} = p_{\mathsf{G}} \cdot w \cdot h \tag{2.1}$$

$$p_{\mathsf{G}} = C_{\mathsf{R}} \cdot \left(\left(\frac{h}{h_1} \right)^n \left(\frac{w}{h} \right)^m + f_{\mathsf{AR}} \right)$$
 (2.2)

Here, h_1 = 1.0 m is a reference ice thickness. The exponents n and m are empirical values that account for the influence of ice thickness and structure width, respectively. For typical design cases, m = -0.16, and n varies with thickness: n is approximately -0.5 for thin first-year ice (h < 1 m), and n =-0.3 for thicker ice. The $C_{\rm R}$ is the ice strength coefficient, also referred to as the global effective crushing strength. It represents a conservative upper-bound estimate of the maximum ice pressure based on full-scale data. An additional shape factor term $f_{\rm AR}$ reduces pressure for wide structures and is shown in Equation (2.3).

$$f_{\rm AR} = e^{-\frac{w}{3h}} \sqrt{1 + 5\frac{h}{w}} \tag{2.3}$$

With this correction, the global pressure better accounts for the multi-directional confinement experienced when ice interacts with a narrow structure, resulting in a higher load (Määttänen & Kärnä, 2011).

It is important to note that $C_{\rm R}$ is not a direct material property that can be obtained from a laboratory strength test. It is an effective crushing strength that averages over the complex failure process, where spalling and splitting can also occur across the entire structure width. In ISO 19906, using these $C_{\rm R}$ values in Equation (2.2) is intended to give a conservative estimate of the maximum global ice pressure expected on a rigid vertical structure in that climate. The empirical correction factors $(h/h_1)^n$ and $(w/h)^m$ in the equation further ensure the formula matches the observed trend that larger contact areas yield lower average pressures.

2.4.1. Site-Specific Scaling of C_R

As previously stated, default C_R values are based on historical data from specific regions, so they must be adjusted when designing wind turbines in new locations with different ice conditions. ISO 19906

proposes options to adjust C_R to better reflect local conditions. These scaling methods are included in the non-normative annex. This part of the standard serves as guidance only. It does not give a complete or prescriptive method for scaling. Instead, it outlines general steps that can be followed when site-specific data is available. Two main options are provided:

- When no detailed site data is available, C_R can be selected based on climate conditions. ISO suggests default values for Arctic, sub-Arctic, and Temperate regions using the amount of Freezing Degree Days (FDD) as a reference.
- When strength-related data is available, ISO proposes scaling using a strength ratio. This allows C_R to be adjusted based on local ice properties or measurements.

The following sections explain these two approaches in detail. It should be noted that the scaling methods proposed in this study are focused on changing the $C_{\rm R}$ values based on the ice strength index. ISO also proposes changing the value of $C_{\rm R}$ for other parameters such as the exposure to ice events, ice drift speed and structure compliance. These factors are not included in this work, but should not be neglected for design purposes.

1. Direct Assignment Based on Climate Conditions

When no local ice strength or property data is available, ISO 19906 recommends selecting a default C_{R} value based on the climate severity at the site. This is determined using the number FDD. The FDD are the cumulative days below freezing over the winter season. Higher FDD values generally indicate colder climates and stronger ice. Freezing Degree Days are calculated as:

$$FDD = \sum_{i=1}^{N} \max(0, T_{f} - T_{air,i})$$
 (2.4)

Where:

- Tair,i is the average daily air temperature [°C],
- $T_{\rm f}$ is the freezing point of seawater,
- $\bullet \ N$ is the number of days in the winter season.

Only days with an average temperature below freezing contribute to the FDD total. The FDD value is used to assign the climate zone and corresponding $C_{\rm R}$ value. These values shown in Section 2.4.1 are intended to provide conservative estimates of global ice pressure for design purposes (ISO19906, 2019). These values correspond to extreme annual events with a 1% probability of exceedance. Other studies that investigate factors influencing the value of $C_{\rm R}$ are discussed in Section 2.4.4.

 Table 2.1: Suggested default $C_{R,0}$ values based on Freezing Degree Days, including example locations (ISO19906, 2019).

Climate Region	Default C_{R} [MPa]	FDD [-]	Example Locations
Temperate	1.8	1000	Baltic Sea, Bohai Sea, Cook Inlet,
			North Caspian Sea
Sub-Arctic	2.4	2000	Okhotsk Sea
Arctic	2.8	4000	Beaufort Sea

2. Strength ratio method

If more ice data is available for the area of interest, ISO 19906 proposes scaling the reference C_R by the ratio of the ice strength index obtained at the specific area of interest and a reference ice strength index, shown in Equation (2.5).

$$C_{\mathsf{R},\mathsf{s}} = C_{\mathsf{R},\mathsf{0}} \cdot \frac{\sigma_{\mathsf{s}}}{\sigma_{\mathsf{0}}} \tag{2.5}$$

where $C_{\text{R,0}}$ is the strength coefficient for the reference region, either Arctic or temperate region. σ_{S} is the measured strength index for the specific area of interest. σ_0 is the measured or inferred strength index for the reference region. This ratio is further explained in Section 2.4.2.

According to ISO, the strength index σ can include various compressive strength measurements. For example, uni-axial/multi-axial strength tests, continuous indentations tests, BHJ tests, or an estimate based on brine volume. In this study, the BHJ method is used to determine the ice strength index, σ . The ice strength at the site of interest and the reference site is represented by $\sigma_{\rm BHJ,s}$ and $\sigma_{\rm BHJ,0}$, respectively. The chosen strength index method must be the same between specific area of interest and reference area (ISO19906, 2019). For example, when conducting BHJ tests, the BHJ used at reference location A should match the geometry and indentation rate of the jack used in location B, to allow for scaling and comparison between sites.

ISO 19906 also describes an alternative method for estimating the ice strength index, which can be used directly to obtain the scaled ice strength coefficient $C_{\rm R,s}$. In this method, the ice sheet is modeled as a set of discrete horizontal layers, each characterized by local temperature and salinity values. These parameters influence the brine volume fraction, $v_{\rm b}$, which affects the mechanical properties and thus the strength of sea ice. Caution is advised by ISO when the local ice temperature or salinity differs largely from the reference climate.

The average strength index, $\sigma_{\rm Bri}$, for a layered ice profile is calculated using the root-mean-square of the strength coefficients. The coefficient, $C_{\rm Bri,i}$, is determined for each layer based on the ISO brine volume-strength relationship. The total number of layers is given by n. The calculation is shown in Equation (2.6).

$$\sigma_{\mathsf{Bri}} = \sqrt{\frac{1}{n} \sum_{i=1}^{n} (C_{\mathsf{Bri},i})^2} \tag{2.6}$$

Since the goal is to obtain the scaled ice strength coefficient $C_{R,s}$, two distinct strength indices must be considered: the reference strength index, $\sigma_{Bri,0}$, and the local strength index, $\sigma_{Bri,s}$, for the area of interest. ISO 19906 suggests standard reference strength indices for two conditions:

- For Arctic regions, a reference strength coefficient $C_{\rm R}$ of 2.8 MPa corresponds to a reference strength index $\sigma_{\rm Bri,A,0}$ of 2.86 MPa.
- For temperate regions, a lower reference strength coefficient $C_{\rm R}$ of 1.8 MPa corresponds to a reference strength index $\sigma_{\rm Bri,T,0}$ of 2.07 MPa.

If detailed ice temperature and salinity measurements are available from the reference location and area of interest, both the reference $\sigma_{\text{Bri},0}$ and local strength $\sigma_{\text{Bri},s}$ indices can be directly calculated from these measurements. The brine volume fractions for each layer, $v_{\text{b,i}}$, can be converted into strength coefficients, $C_{\text{Bri,i}}$, by using the values from Table 2.2. These data points can be interpolated by using Figure 2.3 to obtain a specific $C_{\text{Bri,i}}$ for each layer.

Table 2.2: Ice-strength coefficient C as a function of brine volume $v_{\rm b}$ (from ISO 19906, Table A.8-5).

v_{b}	0.001	0.010	0.025	0.050	0.100	0.200
C_{Bri} [MPa]	8.4	6.0	3.4	1.6	1.0	0.8

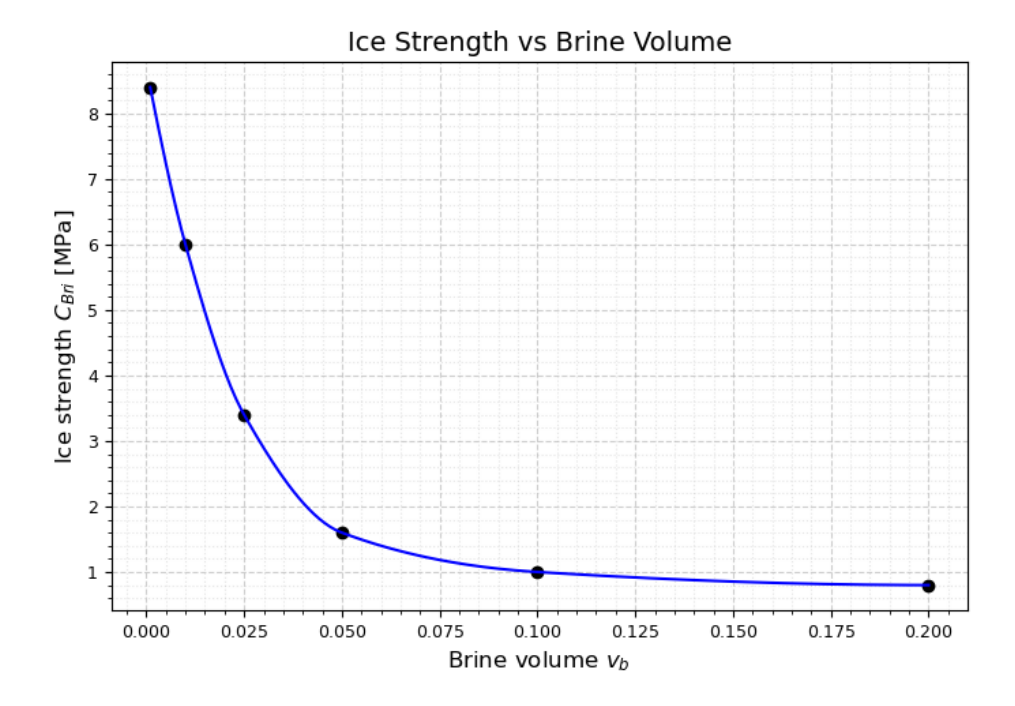


Figure 2.3: Interpolated ice strength coefficient $C_{\rm Bri}$ vs brine volume $v_{\rm b}$, based on ISO 19906 data.

Brine Volume Estimation

The brine volume, $v_{\rm b,i}$, in the sea ice must be calculated to determine the strength index for each layer, $C_{\rm Bri,i}$, which in turn influences the calculation of the overall ice strength index $\sigma_{\rm Bri}$. Since offshore wind turbines may be located in regions where sea ice forms at higher temperatures and lower salinities compared to severe arctic conditions, different methods to obtain the brine volume can be used.

Warm Ice -2 $^{\circ}$ C \leq **T** \leq **0** $^{\circ}$ C When the temperature of ice rises above -0.5 $^{\circ}$ C, the brine volume estimations become less accurate due to the absence of solid salts. For these warmer ice temperatures, Leppäranta and Manninen (1988) researched the method based on thermodynamic equilibrium from the UNESCO standard (Hole, 1978). This UNESCO method takes the following assumptions:

- All salts are dissolved in the liquid brine; no solid salts are present.
- The brine is in thermodynamic equilibrium with the surrounding ice, meaning that $T_{\sf measured} = T_{\sf f}$.
- ullet The bulk ice salinity S remains constant over the temperature range considered.

The brine salinity S_b corresponding to a given ice temperature should be calculated and can be found by assuming thermodynamic equilibrium. The relation between T_f and S_b is given by the UNESCO freezing point in Equation (2.7).

$$T_{\rm f} = -0.0575 \cdot S_{\rm b} + 1.710523 \times 10^{-3} \cdot S_{\rm b}^{1.5} - 2.154996 \times 10^{-4} \cdot S_{\rm b}^{2}$$
 (2.7)

Equation (2.7) must be solved numerically for $S_{\rm b}$, using the measured ice temperature as input for $T_{\rm f}$. Once $S_{\rm b}$ is known, the brine volume fraction based on the UNESCO method, $v_{\rm b,u}$, can be calculated using Equation (2.8).

$$v_{\mathsf{b},\mathsf{u}} = \frac{S}{S_{\mathsf{b}}} \tag{2.8}$$

Where S is the measured ice salinity in ppt. This equation assumes that all the salt in the ice is contained in the liquid brine. At -2 °C, the difference between this method and the one proposed by Cox and Weeks (1982) is minimal (Leppäranta & Manninen, 1988).

Cold Ice ($-22.9\,^{\circ}\mathrm{C} \leq T \leq -0.5\,^{\circ}\mathrm{C}$) For colder ice temperatures, Frankenstein and Garner (1967) proposed equations based on Assur (1960) brine-volume tables. These equations provide brine volume estimates for the following temperature ranges:

$$v_{\rm b,f} = S\left(\frac{52.56}{|T|} - 2.28\right) \quad \text{for } 2.06^{\circ}\text{C} \le T \le -0.5^{\circ}\text{C}$$
 (2.9)

$$v_{\rm b,f} = S\left(\frac{45.917}{|T|} + 0.930\right) \quad \text{for } -8.2^{\circ}\text{C} \le T \le -2.06^{\circ}\text{C}$$
 (2.10)

$$v_{\rm b,f} = S\left(\frac{43.795}{|T|} + 1.189\right) \quad \text{for } -22.9^{\circ}\text{C} \le T \le -8.2^{\circ}\text{C}$$
 (2.11)

For the whole temperature range, Equation (2.12) can be used when less accuracy is needed (Frankenstein & Garner, 1967). ISO 19906 also includes Equation (2.12) in the standard as a general equation to estimate the brine volume.

$$v_{\text{b,is}} = S\left(\frac{49.185}{|T|} + 0.532\right)$$
 (2.12)

The brine volume equations included in Frankenstein and Garner (1967) assume an ice density of 0.926 g/cm³. If the actual ice density (ρ_{ice}) differs significantly, a correction Equation (2.13) should be applied (Cox & Weeks, 1982).

$$v_{b,\text{corr}} = v_{\text{b}} \times \frac{\rho_{\text{ice}}}{0.926} \tag{2.13}$$

By applying these methods to each layer of the ice profile and using the corresponding temperature and salinity measurements, both the reference $\sigma_{\text{Bri,0}}$ and specific area of interest $\sigma_{\text{Bri,s}}$ strength indices can be determined with Table 2.2 and Equation (2.6).

2.4.2. Reduction Factor R

The strength index for the area of interest and can be either higher or lower than that of the reference region. To simplify this increase or decrease, the ratio in Equation (2.5) is referred to as the reduction factor, R, shown in Equation (2.14).

$$R = \frac{\sigma_{\rm S}}{\sigma_0} \tag{2.14}$$

This factor describes how much weaker or stronger the ice at the area of interest is compared to the reference area according to the chosen strength index method. It is then used to scale the strength coefficient with Equation (2.15).

$$C_{\mathsf{R},\mathsf{s}} = C_{\mathsf{R},\mathsf{0}} \cdot R \tag{2.15}$$

ISO 19906 recommends $C_{\rm R,0}=2.8$ MPa for Arctic regions and $C_{\rm R,0}=1.8$ MPa for temperate regions. These serve as baseline reference values in combination with the reduction factor R. The strength index σ used to compute R can be obtained from different test methods. This study investigates the method based on BHJ measurements, $\sigma_{\rm BHJ}$ and based on brine volume, $\sigma_{\rm Bri}$. The two reduction factors are defined in Equation (2.16) and Equation (2.17) and used in this study.

$$R_{\rm BHJ} = \frac{\sigma_{\rm BHJ,s}}{\sigma_{\rm BHJ,0}} \tag{2.16}$$

$$R_{\rm Bri} = \frac{\sigma_{\rm Bri,s}}{\sigma_{\rm Bri,0}} \tag{2.17}$$

 σ_0 refers to the strength of the reference region, while the numerator, σ_s corresponds to the site of interest, e.g., Hjellbotn.

ISO states that brine-based and BHJ-based strength indices follow a similar dependency on temperature and salinity. In other words, when brine volume increases due to warmer temperatures or lower salinity, both $\sigma_{\rm Bri}$ and $\sigma_{\rm BHJ}$ are expected to decrease. This suggests that the corresponding reduction factors $R_{\rm BHJ}$ and $R_{\rm Bri}$ should follow the same trend. If both methods are applied consistently across sites, an open question remains whether the reduction factors can be considered approximately proportional as shown in Equation (2.18).

$$R_{\mathsf{A}} \approx R_{\mathsf{B}}$$
 (2.18)

This assumption is examined further in this work by comparing the two methods in case studies at Hjellbotn and Svea. A guideline to follow when scaling C_R is shown in Figure 2.4.

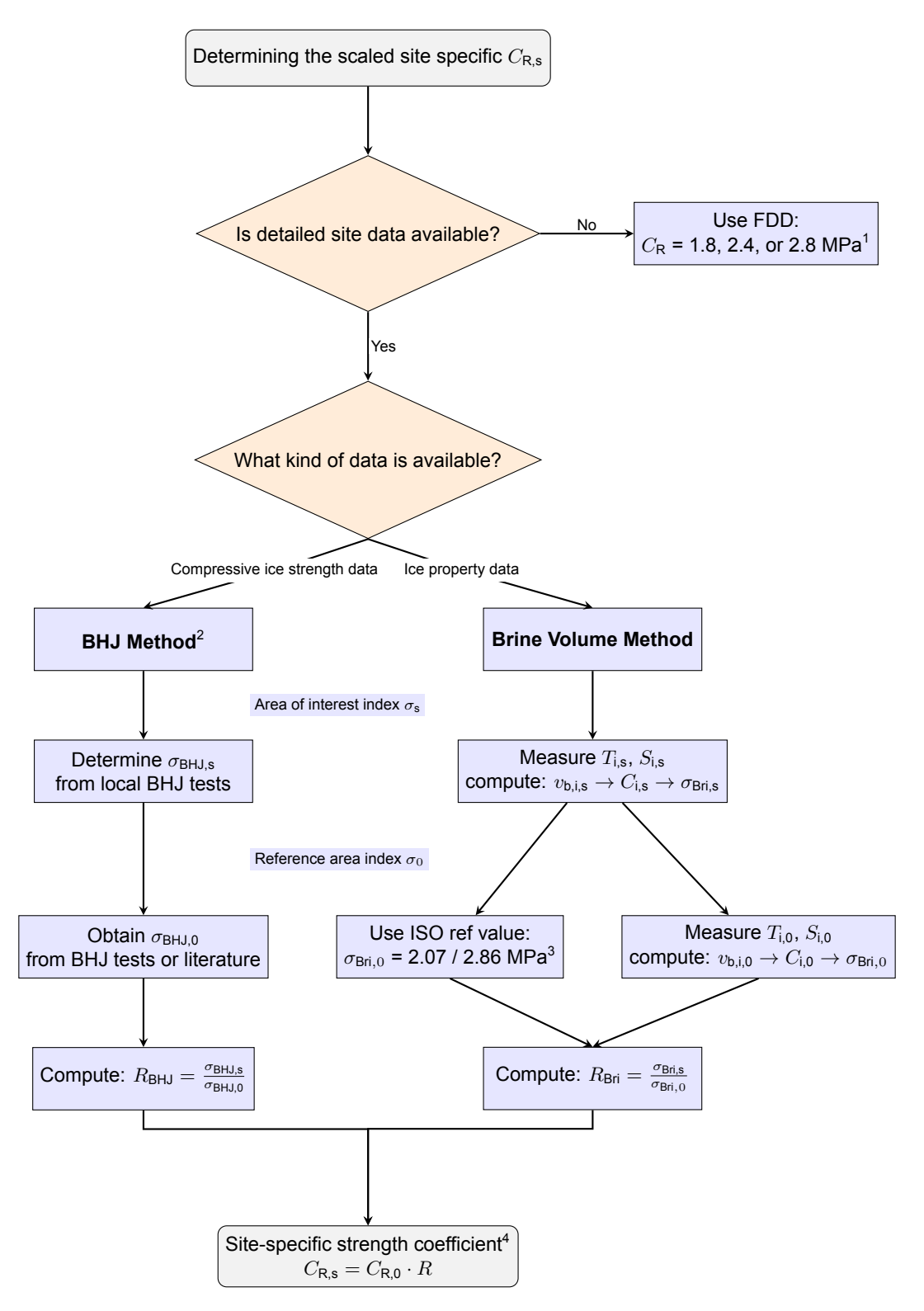


Figure 2.4: Vertical decision flowchart for scaling the ice strength coefficient C_R using ISO 19906. If the brine volume method is used, $\sigma_{Bri,0}$ can be either taken from ISO or calculated from a reference profile.

¹1.8 MPa corresponds to 1000 FDD per winter season, 2.4 MPa to 2000 FDD, and 2.8 MPa to 4000 FDD.

²ISO also proposes other strength measurement methods (e.g., uniaxial/multiaxial tests, continuous indentation), but BHJ is shown here due to its explicit mention in ISO and its use in the case study.

 $^{^3\}sigma_{\mathrm{Bri},0}$ is proposed in ISO as 2.07 MPa for C_{R} = 1.8 and 2.86 MPa for C_{R} = 2.8.

 $^{{}^4}C_{\mathsf{R},0}$ is the C_R coefficient of the chosen reference area, either temperate or Arctic.

2.4.3. Limitations in the standard

The scaling of local ice strength values to derive a site-specific strength coefficient $C_{\rm R,s}$ is supported by ISO 19906. However, the standard provides only general guidance and contains several important limitations that introduce uncertainty when applying its methods. It is important to note that the scaling methodology is found in Annex A, the non-normative part of the standard. This annex is intended to provide optional guidance and support, not strict rules. It is not a complete procedure and requires interpretation by the user. This flexibility makes it difficult to compare results consistently or to validate the method against measured field data. ISO also does not disclose how the Arctic and Temperate reference strength values were derived. The standard provides $\sigma_{\rm Bri,A,0}$ = 2.86 MPa and $\sigma_{\rm Bri,T,0}$ = 2.07 MPa, but does not specify the regions, datasets, or ice types used to derive these values.

Another significant limitation lies in the temperature sensitivity of the brine volume method. While ISO warns that scaling should be done with caution when large differences in temperature and salinity exist between the local site and the reference region, it does not define what qualifies as a "large difference." This makes it difficult to assess whether the scaling method is appropriate in marginal or warm ice conditions. Near the melting point, small measurement uncertainties in temperature or salinity can cause disproportionately large errors in the calculated brine volume and thus the derived strength index. This sensitivity is not fully addressed in the standard's guidance. ISO19906 implies that the scaling method may hold as long as the same testing method is used in both sites. Studies by Paquette and Brown (2017) and Schwarz and Jochmann (2009) show that ice compressive strength is highly variable and sensitive to salinity and temperature. It follows roughly an inverse relationship, as ice warms and brine volume increases, strength drops dramatically. This means that obtaining a representative σ for a site is not straightforward. The ISO standard provides the Equation (2.6) to compute $\sigma_{\rm Bri}$ from profiles, but in practice obtaining detailed temperature/salinity profiles and using them for design is complicated. Moreover, the standard does not explain how to combine multiple measurements or how to treat statistical uncertainty in σ .

ISO also states that data used for scaling should be collected from a "large enough geographic area to be representative". However, it provides no definition or criteria for what constitutes a sufficiently large area. This creates ambiguity when selecting data for regional scaling, especially in environments with high spatial variability in ice properties.

The influence of structural characteristics on measured ice pressures also limits the applicability of the scaling method proposed in the standard. The standard explicitly states that "ice pressures due to continuous crushing obtained on a rigid structure in one region should not be used directly for compliant structures" and adds that pressures on compliant structures can be significantly higher. This highlights a risk when transferring strength indices between applications. Since this thesis focuses only on ice strength obtained with brine volume estimates and BHJ tests, the interaction with flexible structures and the effect of structural compliance is not addressed. This limitation is particularly relevant for offshore wind turbines, which are typically slender and compliant. Most empirical ice pressure data in ISO 19906 originates from stiff oil and gas structures. Applying these data directly to wind turbines without considering their dynamic response and flexibility may result in non-conservative estimates of ice loads. Therefore, applying a scaled ice strength coefficient derived from a rigid reference structure to a flexible wind turbine may underpredict the actual load, even if the scaling is technically correct.

ISO emphasizes that any use of scaling relationships must be supported by proper justification. It warns that "considerable caution should be exercised" when applying scaling methods, particularly when large differences in ice conditions or temperatures are present between the reference and local sites. However, as noted, the standard does not provide specific thresholds, examples, or procedural steps for assessing these differences or for modifying the scaling accordingly. These limitations show that there is a need for careful interpretation of ISO 19906 when applying its scaling methods, especially in non-Arctic, brackish, or variable ice environments. In this thesis, the methods are applied for comparison and analysis purposes only. The resulting $C_{\rm R}$ values are not proposed for direct design use without further consideration of structure-ice interaction effects and regional/seasonal ice variability.

2.4.4. Implications of the $C_{\rm R}$

Several studies have shown the challenges and implications of the ISO 19906 approach to $C_{\rm R}$:

Gravesen and Kärnä (2009) applied ISO 19906 methods to the southern Baltic, a temperate ice area, to determine an appropriate C_R for offshore wind turbine design. Using statistical analysis of the Norströmsgrund lighthouse in the Baltic Sea, they found that the upper-bound effective strength in the northern Baltic of about 0.96 MPa should be reduced by a factor of 0.784 for the milder southern Baltic conditions (Gravesen & Kärnä, 2009). This yielded an estimated $C_R \approx 0.75$ MPa for the Southern Baltic. In other words, the ice in that region was effectively only 40% as strong as the nominal ISO temperate value of $C_R = 1.8$ MPa. The authors noted that ISO's recommended $C_R = 1.8$ MPa, which was based on more severe ice conditions and some built-in velocity effects, would be overly conservative for the Southern Baltic. They also considered the velocity effect on crushing: local data from the Norströmsgrund lighthouse indicated that ice moving very slowly can cause higher local pressures. By accounting for this 20% increase, Gravesen and Kärnä raised the southern Baltic C_R estimate from 0.75 to about 0.90 MPa. Even then, this is only half of ISO's C_R = 1.8 MPa. Their work shows how much regional calibration can influence the design loads. It also shows the difficulty: one must decide how to factor in phenomena like speed effects or structural compliance. The standard itself notes these issues but does not quantify them, so Gravesen and Kärnä had to make assumptions (20% velocity magnification) based on expert judgment. This example shows that, without proper guidance, applying ISO 19906 to a new site can lead to significantly different C_R values.

Lemström et al. (2022) conducted model-scale experiments to investigate ice-structure interaction under controlled conditions. They found that the global ice load on the structure did not increase in proportion to the ice strength. In their tests, the weakest model ice with about half the strength of the strongest ice actually produced higher loads on the structure than the stronger ice did. This counterintuitive result is due to a change in failure mode: the weak ice failed by forming a slushy, dense pile in front of the structure, whereas the stronger ice formed distinct blocks and caused some to buckle or divert the load. The implication for ISO's $C_{\rm R}$ is important: simply having a higher ice crushing strength, due to, for example, a colder temperature, does not always mean the global force will be higher. Other factors like the failure process, rubble formation or ice-structure friction can govern the load. Thus, a single parameter $C_{\rm R}$ cannot capture all situations.

Paquette and Brown (2017) reviewed measured ice crushing pressures and highlighted how test scale and failure modes significantly affect results. The variability in ice pressures depends largely on two main crushing modes: intermittent crushing and continuous brittle crushing. At low speed, intermittent crushing occurs. The ice contacts the structure and causes it to deflect elastically. Over time, the ice establishes full contact across most of the structure's width, while the load on the structure continues to build. Eventually, the ice fails simultaneously over the entire width (full spatial synchronization). At that point, the ice breaks away, the structure springs back, and the process repeats. Continuous brittle crushing, on the other hand, occurs at higher ice velocities. In this mode, spatial synchronization is limited, meaning the ice does not fail simultaneously across the structure. Instead, localized failures occur independently at different points along the width. This results in lower overall peak loads, compared to intermittent crushing.

2.4.5. Probabilistic approach of $C_{\rm R}$

The deterministic approach using predefined coefficients and a single value for $C_{\rm R}$, can lead to unsafe and unreliable designs for new areas with limited historical data. Consequently, a probabilistic approach to determining the $C_{\rm R}$ coefficient can be considered, particularly when the area of interest falls outside the predefined regions from ISO 19906. The standard mentions treating $C_{\rm R}$ as a random variable but does not provide detailed guidance for such implementation (Thijssen et al., 2014). Thijssen and Fuglem (2015) developed a probabilistic methodology to evaluate seasonal ice loads using Monte Carlo simulations based on the ISO formulas. Instead of using a fixed $C_{\rm R}$ = 1.8 MPa, they introduced variability into $C_{\rm R}$ to reflect different ice conditions. Their analysis suggested that a realistic annual characteristic $C_{\rm R}$ for first-year sea ice in the Baltic region could be around 1.34 MPa, lower than the default ISO value of 1.8 MPa. They concluded that the lower probabilistic value already captures effects such as intermittent crushing. This offers a more realistic basis for typical annual ice loading conditions. Similarly, Samardžija (2024) proposed a probabilistic model for assessing ice loads on offshore structures. Their approach also included Monte Carlo simulations. They treated factors like ice ridge size, ice strength, and contact area as random variables. The authors argued that relying solely on deterministic methods with fixed high values of $C_{\rm R}$ can result in overly conservative designs

that overlook important variations in the ice environment. By explicitly modeling these uncertainties, probabilistic methods can better estimate the actual risks of extreme loads and offer potential cost savings in structural design.

3

Method

This chapter describes the methodology used to investigate whether site-specific $C_{R,s}$ values can be derived from local ice strength measurements. Two field campaigns were conducted at Hjellbotn and Svea during the winter of 2025. At each site, confined compressive strength was measured using the BHJ, and ice property data, including temperature and salinity profiles, was collected.

The BHJ used in this study is the latest mechanical jack developed for the NTNU at M-Tech. A dedicated calibration rig was constructed to ensure the accuracy of the load measurements. The calibration process is detailed in Section 3.3.2. Strength estimates based on salinity and temperature were calculated using the method described in ISO 19906. This allowed us to compare the mechanical measurements and environmental property-based predictions.

3.1. Approach

This study investigates the applicability of the ice strength coefficient scaling method proposed in ISO 19906 for deriving a site-specific value of $C_{\rm R}$. For the brine volume method, ISO provides reference values for Arctic and temperate regions, suggesting that local measurements of brine volume are sufficient to obtain a scaled ice strength coefficient, $C_{\rm R,s}$. However, no such reference strength is provided for the BHJ method, which introduces uncertainty when applying this approach at new sites. To evaluate whether the $C_{\rm R}$ scaling approach yields consistent results using both methods, two field sites were selected. Hjellbotn, a temperate fjord in central Norway, was chosen due to its predictable seasonal ice cover and accessibility from the NTNU. The site features warm, brackish, first-year sea ice, which serves as a suitable proxy for the future ice conditions expected at offshore wind turbine sites in the Baltic Sea or similar marginal ice zones. Svea, located in the Van Mijenfjord on Svalbard, was selected as the Arctic reference site due to its well-documented cold-region ice conditions and logistical accessibility through UNIS.

At each site, multiple BHJ tests were carried out and ice cores were retrieved for salinity and temperature profiling. For each BHJ core, the highest measured strength was used in the analysis. This value is considered the best representation of the compressive ice strength during ice-structure interaction. Fieldwork in sea ice environments requires robust and reliable equipment. The instruments must be simple in design, with minimal components that are easy to repair or replace. Portability is also important, as equipment must often be transported over the ice by foot or snowmobile. All equipment should function reliably under freezing temperatures and tolerate snow, slush, and water ingress. Ideally, devices should be operable while wearing gloves and be user-friendly, so they can be used by different team members with minimal instructions. The BHJ device used in this study is mechanically driven and was specifically calibrated for this study. The calibration runs were performed at the NTNU cold lab across different load levels and temperatures to correct for internal friction.

The strength indices based on measured salinity and temperature were calculated using ISO 19906 procedures, detailed in Section 2.4.1. These were compared to BHJ-measured strengths to evaluate whether environmental properties alone can predict the ice strength index accurately, or if direct

mechanical measurements are necessary. By combining results from both methods, the relationship between site-specific ice strength and ISO scaling assumptions is assessed. This approach aims to identify the limitations of the current method and to propose recommendations to improve standard.

3.2. Study Locations

The BHJ tests and supporting ice property measurements at Hjellbotn were carried out by the author in January 2025, with field assistance from K.V. Høyland. The case study at Svea was conducted in April 2025 by students from the University Centre in Svalbard (UNIS) as part of the course "Sea Ice Mechanics and Physics". The data were processed by the author.

3.2.1. Hjellbotn, Norway

Hjellbotn, located in the northern part of the TrondheimFjord in Norway, was selected as the first field site. The site offers consistent seasonal ice formation under fjord-like conditions and provides a safe, logistically accessible place for repeated mechanical testing. It can also be considered as a representative location with brackish, coastal sea ice conditions that may be encountered by offshore wind structures. Hjellbotn is partially isolated from the main TrondheimFjord by two narrow straits, approximately 300 m and 600 m wide, which reduce ocean mixing and promote the formation of a stable surface water layer. A topographic overview is shown in Figure 3.1a.



Figure 3.1: An overview grid of the location of the Hjellbotn area. Retrieved from: Google Earth, 2023
Landsat/CopernicusDataSIO, NOAA, U.S.Navy, NGA, GEBCO IBCAO a: A view of Scandinavia and a part of Europe showing the location of the Fjord with a blue marker. b: A zoomed in view of part of Norway, showing the location of Hjellbotn in the TrondheimFjord, c: A view of the northern part of the Trondheimfjord, with red circles highlighting the small canals that connect Hjellbotn to the larger Fjord. d: A 3D view of Hjellbotn. From (Wilmink, 2024).

An overview of Hjellbotn's location above Trondheim is displayed in Figure 3.1**b**. The fjord's restricted connectivity is shown in Figure 3.1**c**, marked by the two red circles. A detailed 3D view of the location is shown in Figure 3.1**d**. The remaining part of the Trondheim Fjord rarely freezes due to the higher salin-

ity and the influence of the North Atlantic Current, which results in average winter water temperatures of 3-8 °C. However, Hjellbotn still freezes almost every winter. This is due to its sheltered geography and freshwater inflow from surrounding rivers and precipitation. Ice formation typically begins in December or January and lasts for 3-5 months (Høyland et al., 2025). Its proximity to Trondheim and predictable freeze-up pattern make it suitable for fieldwork with the BHJ and ice core sampling for laboratory analysis.

Observations from recent years have shown that the ice in Hjellbotn forms in a low-salinity surface layer, generally 0.5 to 1 m deep, with salinities typically below 1 ppt (Høyland et al., 2025). Snowfall and rain events play a major role in ice formation. Most of the seasonal growth occurs from the top, as snow loads depress the ice and cause flooding. The resulting slush refreezes forming granular or snow-ice layers. In some years, slush layers persist and do not fully consolidate (Hornnes et al., 2023). Ice thickness during the 2022-2024 seasons ranged from 21 to 50 cm, while competent ice thicknesses are typically between 21 and 31 cm (Høyland et al., 2025).

The ice cover remains nearly isothermal throughout much of the winter. Ice temperatures are often close to $-0.5\,^{\circ}\mathrm{C}$, due to the influence of precipitation, flooding, and relatively low freezing degree days. This complicates the application of standard ice growth models. Despite these challenges, the location offers a well-documented and repeatable environment for evaluating the mechanical behaviour of low-salinity sea ice.

3.2.2. Svea, Svalbard

The second field site used in this study was located near Svea in the inner basin of Van Mijenfjord, Svalbard, further referred to as Svea. Svea's location is shown in Figure 3.2. The fjord is approximately 70 km long and partially protected by the island of Akseløya, which shelters the inner basin from direct wave action and inflow from the open ocean. This leads to calm, cold conditions that enable the formation of stable sea ice from early winter until late spring (Høyland, 2009). The Svea area has been studied in previous field campaigns and is commonly used as a reference site for Arctic first-year sea ice. Ice formation typically begins in December or January, with peak thicknesses ranging from 0.9 to 1.3 m by the end of the season (Teigen et al., 2005). Snow depths vary between 5 and 25 cm, depending on local accumulation and wind direction. The ice is saline, with mid-winter salinities typically in the range of 5-7 ppt.

Although remote Arctic regions like the Beaufort Sea would have offered more direct comparisons to ISO reference conditions, logistical constraints limited the field campaign to more accessible areas. Svea was selected as a representative Arctic site due to its reliable ice cover and proximity to UNIS.





(a) Map of northern Scandinavia showing the study locations. The light blue marker shows the location of Hjellbotn and the pink marker shows Svea in the Svalbard archipelago. Image source: Google Earth, 2023. Data: Landsat/Copernicus, SIO, NOAA, U.S. Navy, NGA, GEBCO, IBCAO

(b) Zoomed-in map of the Svalbard archipelago showing the location of Svea (pink marker) in Van Mijenfjord. Image source: Google Earth, 2023. Data: Landsat/Copernicus, IBCAO.

Figure 3.2: Study area overview maps.

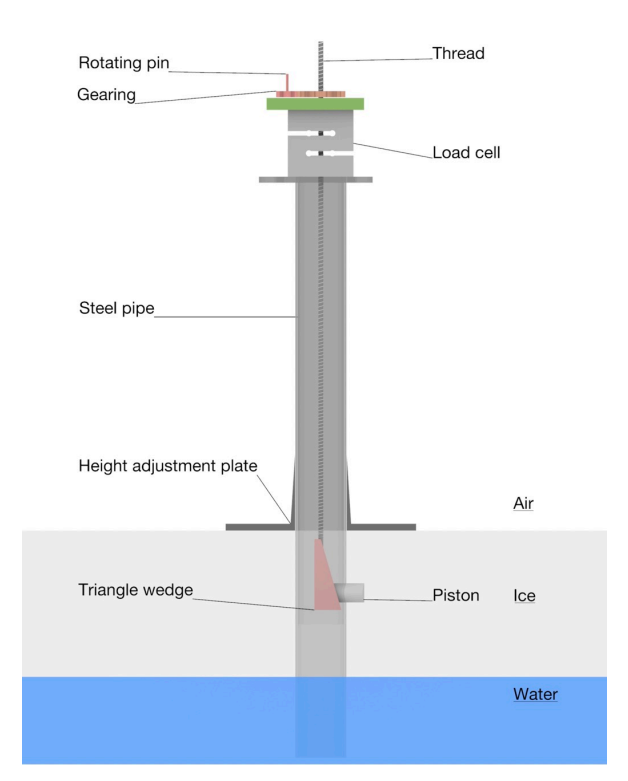
3.3. The Borehole Jack

The BHJ used in this study measures the confined compressive strength of sea ice by expanding a piston radially against the inner wall of a vertical borehole.

3.3.1. Design and Operation

The BHJ was originally developed at CRREL in the 1970s for in-situ ice strength testing (Sinha, 2011). It is designed to measure local ice strength and is compact enough for use in remote field conditions. The version used in this study consists of a steel cylinder inserted into a pre-drilled borehole. Inside the cylinder, a triangular wedge drives a single piston outward. The wedge is connected to a threaded steel rod, which runs vertically through the center of the jack. A handheld Makita DDF486 drill, mounted on top of the housing, rotates a gear which moves the rod upward. A schematic of the internal mechanism is shown in Figure 3.3a.

The top unit contains the gear system, shown in Figure 3.3b. This gear converts the drill's rotation into vertical motion of the threaded rod. As the rod moves upward, it lifts the red wedge, which presses the piston outward. This mechanism provides a controlled and repeatable loading process, suitable for comparing results between different tests.





(a) Side view of the BHJ inserted in an ice sheet. The ice sheet is shown in light grey above the water surface. The red wedge is connected to a threaded rod that extends to the top of the rig. A handheld drill is mounted on the rotating pin at the top, driving the mechanism.

(b) Photograph of the BHJ with the upper plate opened to show the internal gearing system. These gears are normally covered during operation and convert the drill's rotation into an axial movement of the threaded rod.

Figure 3.3: Overview of the Borehole Jack design and mechanics. (a) shows a technical drawing of the jack in an ice sheet, (b) shows the exposed gear system at the top of the unit.

Two axial load cells shown in Figure 3.4a are installed between the top of the steel cylinder and the top unit shown in Figure 3.3b. These cells record the vertical pulling force required to move the wedge upward, which in turn presses the piston outward. Since the wedge transforms vertical motion into horizontal displacement of the piston, the force measured by the load cells is not equal to the force applied to the ice wall. A calibration factor c was used to correct for the wedge geometry and internal friction. The internal friction was minimized by using a dry graphite. Graphite was selected because it maintains a low and consistent friction coefficient under high pressure at sub-zero temperatures (Stachowiak & Batchelor, 2005). The c factor was determined through laboratory testing and is described in Section 3.3.2.

The piston has a maximum extension of approximately 32 mm. During testing, the indentation speed was kept constant by using maximum speed on the drill's slowest setting. This results in a continuous indentation speed of 0.9 mm/s. When fully extended, the piston slides in a groove in the wedge that enables retraction during reverse rotation of the system. The extended and retracted piston positions are shown in Figure 3.4c and d.

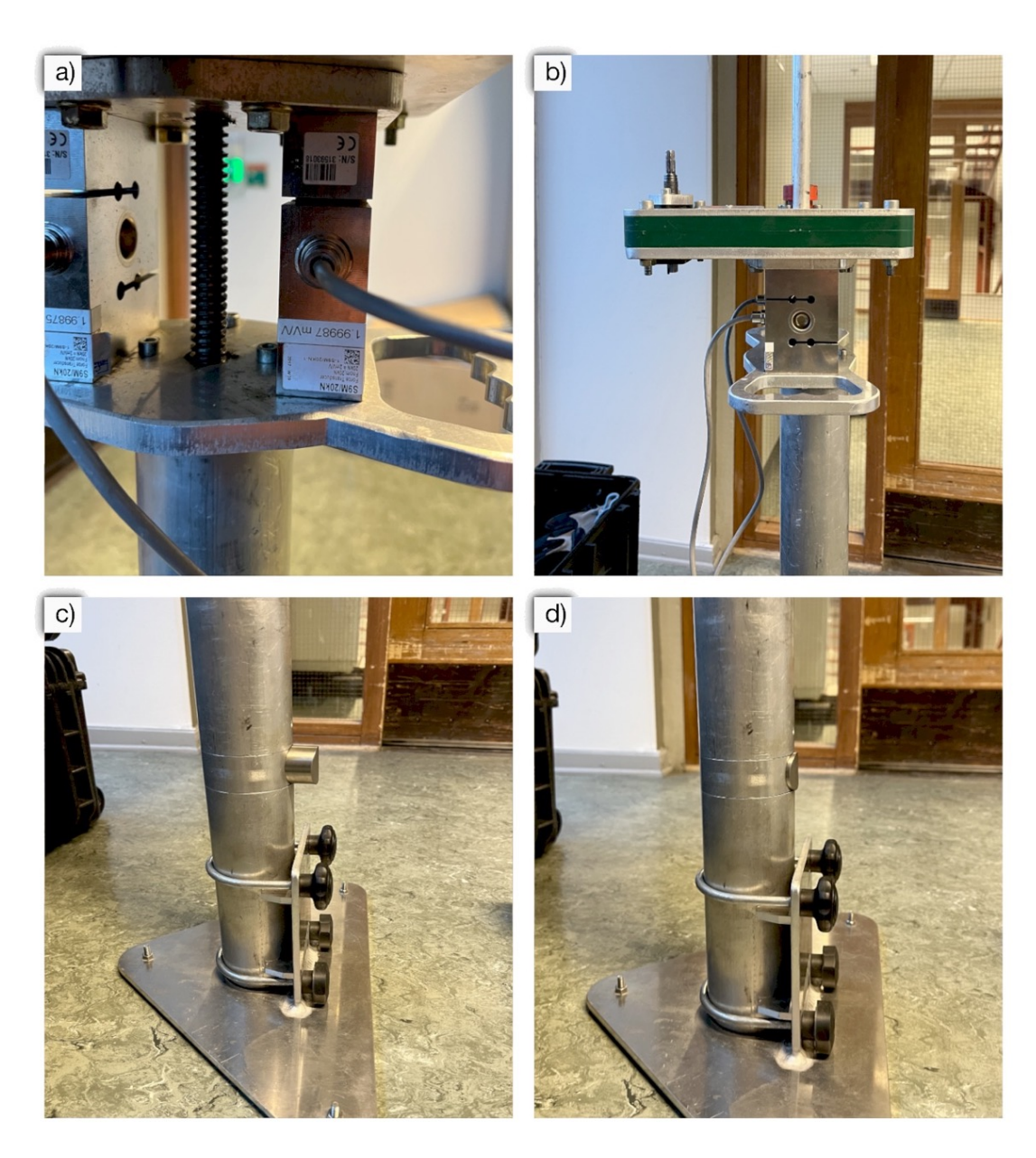


Figure 3.4: Photograph with detailed views of the BHJ. **a**: Load cells and threaded rod. **b**: Gearing system. **c**: Piston extended. **d**: Piston retracted.

The indentation depth of the piston can be adjusted using the steel surface plate. Force data from both load cells is recorded in real time by a data logger connected to a field laptop. This configuration also makes it possible to monitor the load curve during testing. No external power is required, which makes the testing possible in remote areas. A photo of the BHJ during field testing including its transportation case and field laptop is shown in Figure 3.5. During use, only the top control unit remains visible above the ice surface, while the part below the height adjustment plate extends into the ice and water below. All BHJ tests are carried out at an indentation depth of half the total ice thickness. This results in consistent testing conditions and best represents ice-structure interaction, where the middle part of the ice is typically subject to the highest pressure, depending on the internal layering of the ice.



Figure 3.5: Photograph of the BHJ including field laptop, transportation case and logger box in field testing mode.

The maximum load recorded by the sensors, converted using the calibration factor, was used as the representative value for confined compressive strength. This value is referred to as borehole ice strength. While it does not represent uniaxial compressive strength directly, previous studies that have shown it provides a useful and repeatable index for comparing sea ice mechanical behaviour under in-situ conditions (Sinha, 2011).

3.3.2. Calibration

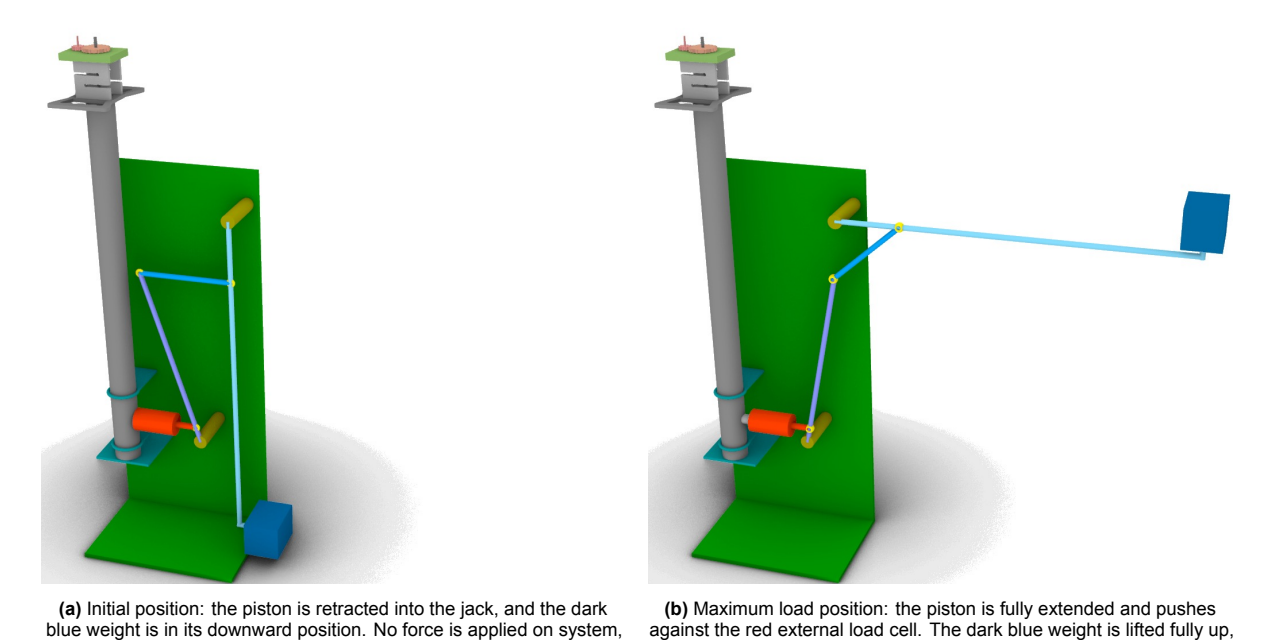
To ensure accurate and consistent strength measurements during field testing, the BHJ requires calibration to determine the relationship between the recorded internal axial force and the actual radial force applied by the piston on the ice. This relationship is expressed with a correction factor c, which converts the vertical pulling force F_{rec} recorded by the load cells into the outward indentation force F_{pist} applied to the borehole wall. The relationship is shown in Equation (3.1).

$$F_{\mathsf{pist}} = c \cdot F_{\mathsf{rec}}. \tag{3.1}$$

The correction factor accounts for both the wedge geometry and internal friction losses. The friction is mainly caused by three interfaces. The surface between the piston and the wedge, between the piston and the housing, and between the wedge and the inner housing.

To determine a suitable c-factor corresponding to the load cases and local temperature conditions in this study, a laboratory calibration rig was developed and tested in collaboration with M-TECH, Trondheim. The setup simulates the internal force transmission of the BHJ under controlled loading. A schematic of the rig is shown in Figure 3.6. It was installed in NTNU's cold laboratory to simulate realistic field

temperatures during calibration. The BHJ is placed inside a housing to restrict horizontal motion, as shown in Figure 3.7a. The piston's outward movement is redirected into a rotational lifting motion using a three-beam linkage system. The first beam, marked in purple in the schematic, is hinged at its base, just below the piston contact point. This purple beam pushes a blue beam sidewards. A third light blue, hinged at the top holds a dark blue counterweight at the bottom. As the piston extends, the beams rotate and lift the counterweight, shown in Figure 3.6b. This results in an increased load on the piston, which represents the loading conditions experienced in ice. The geometry of the calibration rig is shown in Figure 3.6



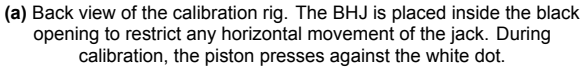
and the red load cell is not measuring any load. resulting in a maximum force being applied on the system. Figure 3.6: Schematic overview of the BHJ calibration setup. (a) shows the unloaded position, and (b) shows the configuration

under full extension.

blue weight is in its downward position. No force is applied on system.

The geometry of the linkage resulted in a mechanical amplification factor of approximately 50 as the beam approached a horizontal position, as shown in Figure 3.6b. The force applied to the piston was measured using a high-precision HBM load cell, as shown in Figure 3.6 in red, placed in line between the piston and the contact point of the first beam. Internal axial forces were recorded simultaneously from the BHJ's load cells shown in Figure 3.6 in light grey just below the light green top plate. The data was stored and synchronized using the LabVIEW software. A picture of the calibration rig is shown in Figure 3.7.







(b) Side view of the calibration rig, including a square cut out for the external load cell. The jack including the Makita drill is placed in the rig and the weight is almost reaching its maximum height.

Figure 3.7: Photographs of the BHJ calibration rig at NTNU. (a) shows the back view where the BHJ is inserted into the rig, and (b) presents a zoomed-in side view with a clear view of the load cell setup.

In previous calibration tests by Kvale et al. (2019), a different approach was used where the piston was pressed directly against a stiff mechanical spring. While this method was compact, it provided very limited piston travel and high initial stiffness. This led to a rapid load buildup and component overstress. With the new counterweight-based system, the reaction force increases gradually which better reflects the force profile experienced during field testing. To minimize friction variability, a graphite-based dry lubricant was reapplied after every ten tests. Graphite was preferred over other lubricants due to its performance under high load and stable, low-friction properties at sub-zero temperatures (Khonsari & Booser, 2008).

To assess the influence of temperature on force transmission, calibration tests were carried out at three temperature levels: $20\,^{\circ}\mathrm{C}$, $-5\,^{\circ}\mathrm{C}$, and $-10\,^{\circ}\mathrm{C}$. The BHJ was acclimatized in the cold room before each test series. For each temperature, ten repeated loading cycles were performed. Between cycles, rest periods of 5 seconds to 3 minutes were introduced to assess the effect of frictional heating. In each case, the correction factor c was computed as the ratio between the peak load measured by the external reference cell and the peak axial force recorded internally. The use of peak force follows the interpretation method applied in BHJ field tests and in previous studies where maximum load values are taken as the representative value (Hornnes et al., 2024; Sinha, 2011). The results of the calibration tests are shown in Section 4.1.

3.4. Ice Property Measurements

Aside from BHJ tests, additional ice properties were obtained at both field sites. These properties included ice thickness, temperature, salinity, and density readings. The properties were used for environmental comparison and for the secondary strength estimation method based on ISO 19906.

3.4.1. Ice Thickness

Ice thickness was measured using a standard Kovacs drilling and gauge kit. At each BHJ test location, a vertical hole was drilled manually, and a hooked measuring tape was inserted to determine the total thickness of the ice cover. Thickness readings were recorded before each BHJ test to determine the indentation depth.

3.4.2. Temperature and Salinity Sampling

At Hjellbotn, the ice temperature was measured with the Edro TFX 410-1 thermometer after retrieval of the core. In addition to core measurements, ice temperature was also recorded using a thermistor string. The string was installed on the day of BHJ testing and remained in place for three weeks. It recorded the vertical temperature profile over time, capturing daily variations in the ice, water and air. A photograph of the installed string is shown in Figure 3.8.

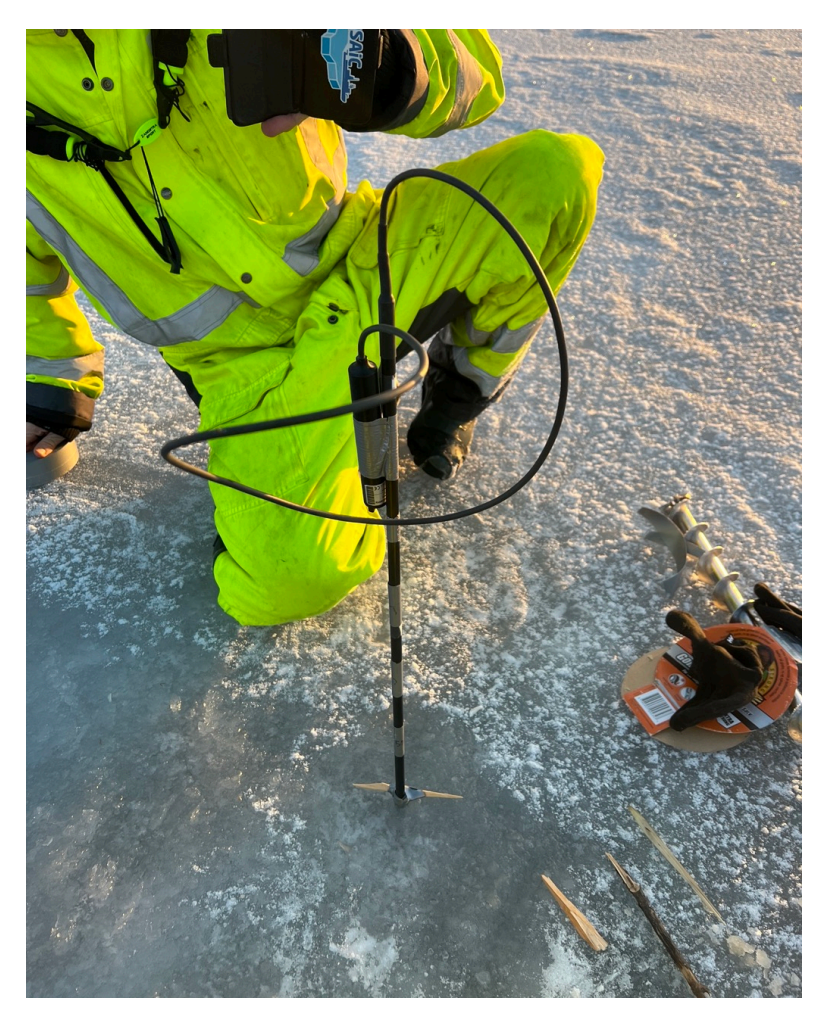
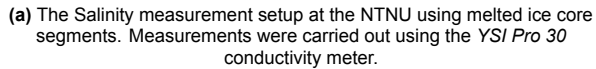


Figure 3.8: Photograph of the thermistor string installed at Hjellbotn to monitor the vertical temperature profile.

At Svea, ice temperatures were measured directly from vertical ice cores. After extraction using a Kovacs Mark III ice coring drill (shown in Figure 3.9b), small holes were drilled into the core at 5 cm intervals, and the thermometer was inserted to a depth of approximately 2 cm. Measurements were taken immediately after extraction.

Salinity measurements were carried out using the same procedure at both sites. Each core was cut into horizontal layers of approximately 5 cm thickness. The segments were stored in sealed containers and melted at room temperature. Once fully melted, the salinity was determined using the YSI Pro~30 handheld conductivity meter with an accuracy of $\pm~0.01$ ppt. This method provides a salinity profile along the full ice column. An image of the salinity testing process is provided in Figure 3.9a.







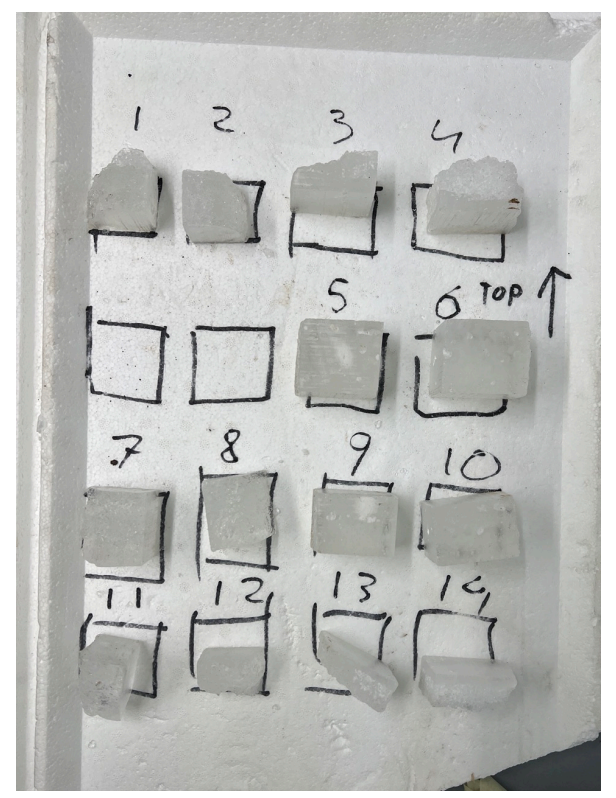
(b) Overview of ice drills. Top left: Kovacs drill for ice thickness. Bottom left: drill for BHJ borehole. Right: drill for ice core extraction. All drills are operated with a Makita cordless drill.

Figure 3.9: Examples of equipment used for ice property measurements and ice strength measurements.

3.4.3. Density measurements

Ice density was measured using the hydrostatic weighing method. This approach results in higher accuracy than the weight-over-volume method (Pustogvar & Kulyakhtin, 2016). To obtain strength estimates based on salinity, ice cores were cut into horizontal layers. The number of layers was limited to a level that was practical for sampling while still providing enough ice volume for reliable salinity measurements.

The ice sample was first cut into layers and then into smaller blocks, typically around 5 cm by 5 cm in size. An example of the prepared samples is shown in Figure 3.10a. The mass of each block was first measured in air using a scale. Then, the block was fully submerged in paraffin and weighed again using the same scale. These measurements were performed in a cold laboratory at a constant temperature of around -15 $^{\circ}$ C. The setup with the ice block submerged in paraffin is shown in Figure 3.10b.





(a) Ice block retrieved at Hjellbotn cut into layers and test blocks.

(b) Hydrostatic weighing setup with submerged block in paraffin.

Figure 3.10: Preparation and Hydrostatic weighing setup in the NTNU cold laboratory.

The density of the paraffin was measured separately using a calibrated aerometer. The ice density could was then calculated using Archimedes principle, as shown in Equation (3.2).

$$\rho_{\rm ice} = \frac{m_{\rm air}}{m_{\rm air} - m_{\rm par}} \cdot \rho_{\rm par} \tag{3.2}$$

where:

- $m_{\rm air}$ is the mass of the ice block in air,
- m_{par} is the mass of the block submerged in paraffin,
- $\rho_{\rm par}$ is the density of the paraffin.

This method is particularly useful for measuring the density of ice below the waterline. During sampling, some brine may be lost from open brine channels or brine pockets. However, paraffin fills these gaps during immersion, preserving volume, which reduces the error. According to Pustogvar and Kulyakhtin (2016), the method has a typical uncertainty of less than 0.2%, making it suitable for detecting small variations in ice density.

Results

This chapter presents the results from the case study carried out in Hjellbotn and Svea. Confined compressive strength measurements obtained with the Borehole Jack are compared between the two sites. The results from the ice property measurements are also presented. The resulting brine volume ice strength index obtained from the salinity and temperature measurements is then compared to the Borehole Jack strength index. The measurements at Hjellbotn were carried out in January 2025, and in Svea in April 2025. At both locations, the ice was in a growing phase and showed no signs of melting.

4.1. Borehole Jack Calibration

The BHJ calibration produced consistent results across the tests where the jack was given sufficient time to acclimatize to the test temperature. The c factors were measured at three temperatures and for three load levels. The tests showed that both temperature and applied load affected the resulting c value of the jack. The results are shown in Table 4.1 below.

Table 4.1: Correction factor c with standard deviation from calibration tests.

Load [kg]	20 °C	-5 °C	-10 °C
10	$\textbf{2.12} \pm \textbf{0.063}$	2.17 ± 0.177	$\textbf{2.75} \pm \textbf{0.118}$
20	1.84 ± 0.059	2.10 ± 0.071	2.50 ± 0.061
30	1.84 ± 0.046	2.04 ± 0.019	2.31 ± 0.001

The results indicate two notable trends. First, the factor c increases as the temperature decreases. This indicates that the graphite lubricant reduces its gliding capabilities at lower temperatures, leading to increased internal friction in the jack mechanism. Second, higher applied loads correspond to slightly lower c factor. This suggests that mechanical efficiency improves under higher force. This may be due to a reduced relative influence of internal friction between the piston and wedge components or other internal friction in the jack.

The BHJ field tests at Hjellbotn and Svea were conducted at temperatures close to -5 $^{\circ}$ C, with recorded loads similar to the load levels observed during calibration with 10 and 20 kg. Based on this, an interpolated correction of c = 2.13 was used. This factor was applied in the BHJ strength analysis for all BHJ measurements.

4.2. Hjellbotn Case Study Results

4.2.1. Ice Conditions

In November, the daily mean air temperature at Steinkjer was still well above freezing, preventing any significant ice formation on Hjellbotn. During December, the temperature dropped and began fluctuating around $0\,^{\circ}\mathrm{C}$. Some periods of melt and freeze followed with the first weeks of January providing a

more consistent drop below freezing (see Figure 4.1). This colder period enabled initial ice formation on Hjellbotn. However, tidal movement strongly influences ice formation near the shore at Hjellbotn. Every 6.25 hours, the ice near the shore is lifted up and down on the beach, breaking it into rubble. A rise in temperature combined with a strong storm in mid-January caused the newly formed ice to break up further and the ice rubble was all pushed ashore. Just after the storm, field access was not possible due to the presence of a wide open-water strip, approximately 30 m in width, between the shoreline and the main ice pack, this can be seen in Figure 4.2a. The rubble pile is shown in Figure 4.2b. The higher than usual air temperatures in December and early January made it also more difficult to access compared to the years before. The surface water temperature during this first visit was measured at $0.5\,^{\circ}\mathrm{C}$. A colder period after this storm allowed the ice to grow and enabled us to safely access the ice just before the end of January.

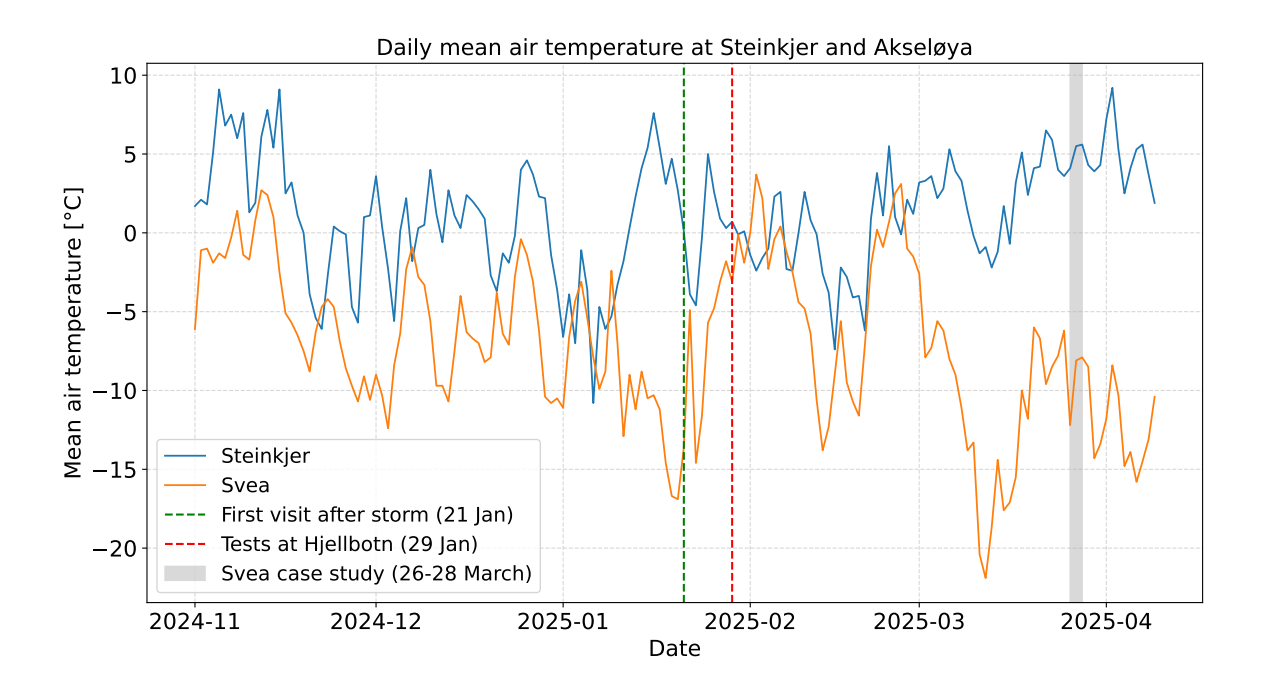


Figure 4.1: Daily mean air temperature at Steinkjer (weather station 11 km from the Hjellbotn test-site, 12.1 m above sea level) and Akseløya (Weather station 40 km from the Svea test-site, 15 m above sea level). The dashed green line indicates the first field visit after a storm at Hjellbotn (21 January 2025). The red dashed line marks the day when the measurements at Hjellbotn were carried out (29 January 2025). The grey zone marks the period when the measurements at Svea were carried out (26-28 March 2025).





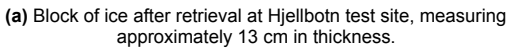
(a) Open water gap between shoreline and ice cover on 21 January after a storm.

(b) Ice rubble near the shoreline caused by a storm forcing ice floes up the beach.

Figure 4.2: Photographs of the shoreline conditions at Hjellbotn during the initial site visit on 21st of January 2025.

During the second visit on 29 of January, the open water had refrozen and a tidal window allowed temporary access to the ice. Safe access was possible for approximately four hours during low tide, when the shore ice was grounded and the pack ice could be reached. The ice consisted of a clear bottom layer and a more porous top layer, likely due to the warmer period with snow melt earlier in January and December. The layers are visible in Figure 4.3.







(b) Sawed block of Hjellbotn ice in the cold lab at NTNU. Retrieved for density measurements.

Figure 4.3: Photographs of the ice layers at Hjellbotn retrieved on 29 January 2025. Distinct stratification is visible, with a solid ice layer at the bottom and a more porous layer at the top.

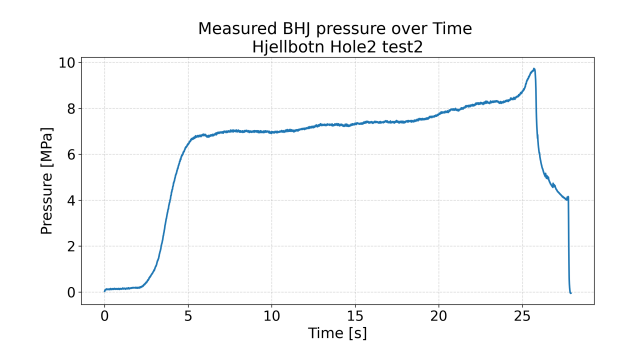
4.2.2. BHJ Strength Measurements

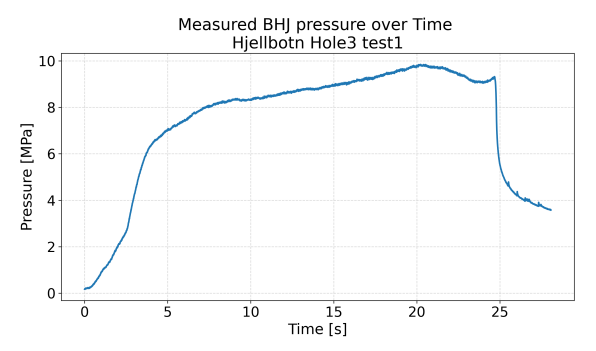
At the Hjellbotn site, six boreholes were prepared and tested with the BHJ. Two strength measurements were taken in each hole. After each test, the jack was rotated either by 90° or 180° before the second indentation. In total, 12 strength values were obtained. The maximum BHJ strength measured over all the tests was 7.40 \pm 1.47 MPa using a calibration factor of 2.13. The individual results are listed in table 4.2.

Table 4.2: Maximum measured BHJ pressure and failure observation for the two tests performed in each hole at Hjellbotn. A calibration factor of 2.13 was used to obtain the BHJ strength.

Hole	Test 1 [MPa]	Test 2 [MPa]	Failure Observation
1	7.26	6.19	Spalling up and down
2	8.03	9.74	No visible spalling
3	9.84	9.72	No visible spalling
4	6.46	6.12	Spalling up
5	6.93	6.44	Spalling up and down
6	6.05	6.03	Spalling down

The tests in holes 2 and 3 did not show any signs of spalling with no visible cracks or chips around the borehole wall. The average strength of these non-spalling tests was 9.33 ± 0.75 MPa. Two tests where no visible spalling occurred are shown in Figure 4.4.





(a) BHJ test in Hole 2, Test 2. The pressure curve shows a sharp increase between 0–5 seconds. This increase transitions into a slower increasing pressure indicating a flow-stress failure mode. Just before maximum piston travel, a sudden spike is observed, with a peak pressure of 9.74 MPa. Visual inspection after the test showed no spalling in the borehole.

(b) BHJ test in Hole 3, Test 1. A sharp pressure increase is observed between 0-5 seconds. After 5 seconds, the pressure follows a less steep increase in pressure indicating an upper yield failure mode. A maximum pressure of 9.82 MPa was observed, followed by a sharp drop when the piston reached its end position. Visual inspection showed no spalling in the borehole.

Figure 4.4: Borehole Jack pressure over time curves from hole 2 and 3 performed at Hjellbotn. Visual inspection confirmed no spalling occurred in either tests.

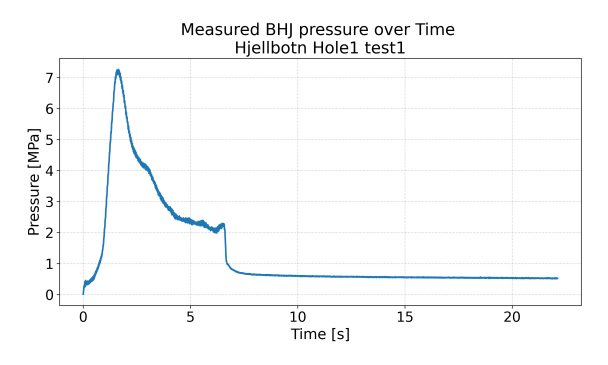
On the other hand, the remaining holes showed clear spalling, either upward or downward, or both. This means that ice fragments detached from the borehole wall during the piston expansion. The premature failure due to spalling was observed in field. Two examples are shown in Figure 4.5, with corresponding pressure plots shown in figure 4.6. The average strength of the spalling tests was lower at 6.44 \pm 0.41 MPa.

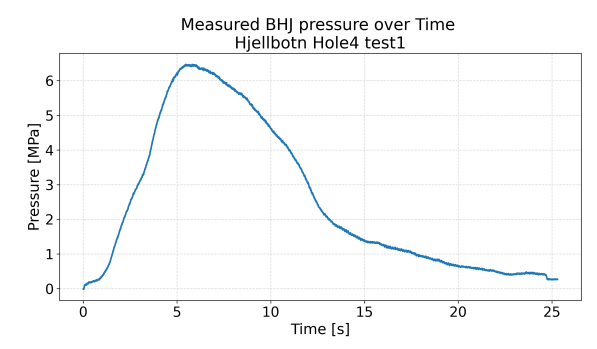




- (a) Photograph of up and downward spalling in hole 1 in both test directions.
- (b) Photograph of hole 4 showing upward spalling observed in both test directions.

Figure 4.5: Examples of spalling after BHJ measurements in Hjellbotn in holes 1 and 4.





- (a) BHJ test in Hole 1, Test 1. The pressure increase rapidly in the first 2 seconds, reaching a maximum pressure of 7.26 MPa, followed by a rapid pressure drop between 2–3 seconds indicating premature failure. Visual inspection revealed spalling both upward and downward.
- (b) BHJ test in Hole 4, Test 1. Between 5–6 seconds, a steep increase in pressure is observed, reaching a maximum of 6.46 MPa before a sharp drop occurs. Visual inspection revealed spalling upwards.

Figure 4.6: Borehole Jack pressure-time curves from Hole 1 and Hole 4 at Hjellbotn, where spalling was observed. Visual inspection confirmed spalling in both tests, upward and downward in Hole 1, and upward in Hole 4.

In the remainder of this study, only the non-spalling tests are used to represent the specific ice strength index at the area of interest, $\sigma_{\text{BHJ},s}$ = 9.33 \pm 0.75 MPa. Spalling indicates local disturbances around the borehole and may lead to an underestimation of the true compressive strength. The tests without spalling are therefore considered to better represent the ice conditions at Hjellbotn. All BHJ response curves are shown in Appendix A.1.

4.2.3. Ice Temperature

During the second visit to Hjellbotn, a thermistor string was installed in the ice to record internal ice temperatures over time. The ice thickness at the thermistor site was measured to be 14 cm at time of installation. The surface water temperature had decreased to 0°C. The average ice temperature

at Hjellbotn during the BHJ tests was approximately -0.2°C. Around 8 February, a short warm period caused the ice temperature to increase. By the end of February, the temperature at the bottom of the ice column had risen to about -0.1°C, while the top remained colder at around -0.4°C. The measurements show that the ice at Hjellbotn remained relatively warm in the first month after testing. The air temperature during this period was approximately -2.5°C. The average ice temperature over the entire thickness of the ice is shown in Figure 4.7. The data corresponds to sensors 12, 13, and 14, which were located in the ice.

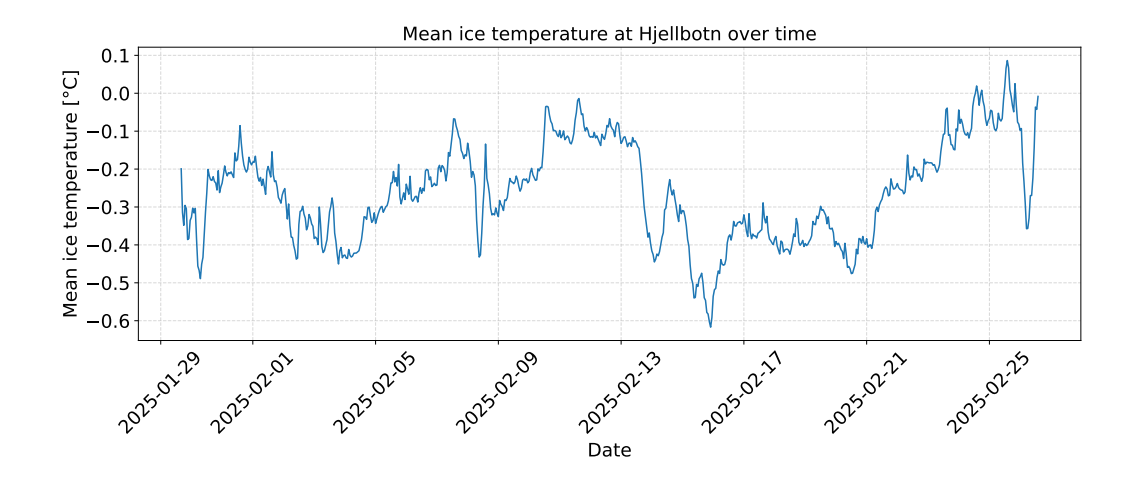


Figure 4.7: Average ice temperatures at Hjellbotn in February 2025, recorded by thermistor sensors 12, 13, and 14 in the 12-14 cm thick ice sheet.

4.2.4. Salinity

Ice salinity was measured from vertical cores taken near borehole 3 and 5 at Hjellbotn. Each core was sliced into horizontal layers about 5 cm thick. The melted samples were analyzed using a handheld conductivity meter. The results of this analysis are shown in Table 4.3.

Hole 3 had salinity values of 0.14, 0.13, and 0.26 ppt from top to bottom. Hole 5 contained salinity levels of 0.12, 0.15, and 0.15 ppt. As visible in Table 4.3, the salinity increased with depth. This trend suggests that the top of the ice may have formed from snow or rainwater, which froze with lower salinity. These differences in layering can be seen in Figure 4.3b. The salinity in the bottom layer of Hole 3 is significantly higher than in the other layers. This can indicate a skeleton ice layer. Ice growth close to shore can be affected by tidal movements and local depth changes which can lead to a high variability in salinity.

Layer	Hole 3 (ppt)	Hole 5 (ppt)	Average (ppt)
1 (top)	0.14	0.12	0.13
2 (middle)	0.13	0.15	0.14

0.26

Table 4.3: Measured salinity values for each layer in ppt from two cores retrieved at Hjellbotn.

4.2.5. Density

3 (bottom)

The ice density was measured at the NTNU cold lab using the hydrostatic weighing method. Two full ice blocks were extracted near Hole 3 and Hole 5. Each block was divided into three horizontal layers of equal thickness. Several test samples were cut from each layer and measured individually. All measurements were performed in the NTNU cold laboratory at -15 $^{\circ}$ C, following the procedure described

0.15

0.21

in Section 3.4.3.

The results are shown in Table 4.4. In Layer 1, the average density was 851 kg/m³. Layer 2 showed a slightly lower average of 836 kg/m³. Bottom layer 3 showed the highest density at 915 kg/m³. The density difference between the layers is clearly visible. The top two layers are less dense, likely due to their formation from refrozen rainwater and snow. These layers contain more air pockets, which results in a lower density. The bottom layer represents the original fjord ice and is denser and more consolidated. These layers are also clearly visible in the retrieved ice blocks, shown in Figure 4.3b. Holes 3 and 5 were located near the shoreline, where tidal action and ice movement had disrupted and broken up the pack prior to testing. This may have influenced the upper layers and contributed to the observed differences in structure.

Table 4.4: Ice density for each layer at Hjellbotn, retrieved from samples of Hole 3 and Hole 5.

Layer	Hole 3 [kg/m ³]	Hole 5 [kg/m ³]	Average [kg/m ³]
1 (top)	845	856	851
2 (middle)	835	837	836
3 (bottom)	915	914	915

4.2.6. Interpretation of Test Results at Hjellbotn

The Borehole Jack tests at Hjellbotn should be interpreted with caution. Only a limited number of measurements were carried out, all close to the shoreline. With just two boreholes not showing spalling after indentation. Later during the fieldwork, the tide had dropped significantly, and the ice was nearly grounded on the beach. This may have affected the stress conditions and the mechanical response of the ice. In all cases, the BHJ was placed in the middle half of the ice thickness. While this is consistent with the Svea measurements, it may have introduced a bias at Hjellbotn by not fully capturing the mechanical contribution of the denser and more consolidated bottom ice layer. The upper part of the ice at Hjellbotn had a lower density and higher porosity. As a result, the BHJ tests may have reflected the weaker properties of the upper ice rather than the full vertical strength profile. However, due to the limited ice thickness, individually measuring the strength of each layer was not possible.

Furthermore, the calibration factor used to convert BHJ pressures into strength values was derived from an interpolated relationship between pressure and temperature based on laboratory tests. This interpolation provided an average calibration factor suitable for both Hjellbotn and Svea conditions. However, such an approach may have reduced the accuracy of the estimated strength values.

Temperature measurements during testing indicated that the ice was close to its melting point, around $-0.2^{\circ}\mathrm{C}$. In this temperature range, small variations lead to large changes in brine volume and mechanical strength. With only two salinity cores available, the reliability of the brine volume estimate is limited. The measured salinity values were very low, suggesting ice close to freshwater conditions — outside the scope of typical saline sea ice for which ISO 19906 is designed. This implies that the brine-based scaling method prescribed by ISO may not be directly applicable here. Moreover, the limited spatial sampling prevented assessment of potential heterogeneity across the site. Visual differences in the ice stratigraphy and known shoreline effects imply that spatial variability was likely, but could not be quantified within the fieldwork constraints.

Figure 4.8 shows the estimated probability of bending versus crushing failure for different ice thicknesses. For the 14 cm thick ice observed at Hjellbotn, the probability of bending failure was higher than that of crushing. This may help explain why spalling was frequently observed during the BHJ tests, rather than uniform indentation.

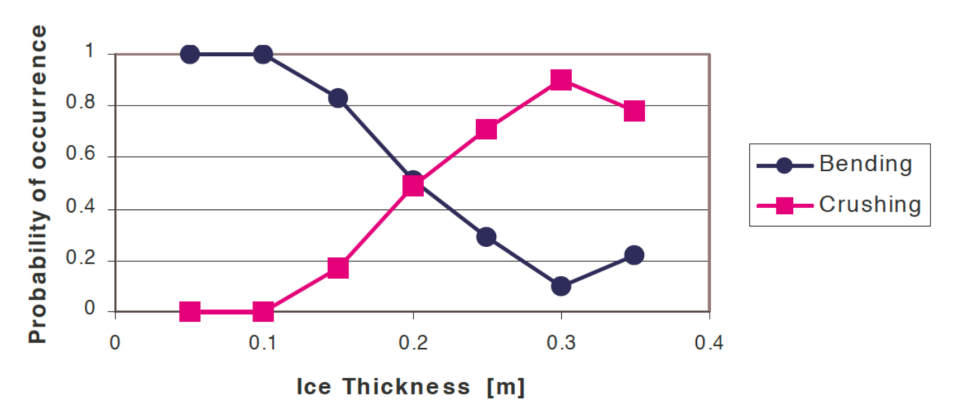


Figure 4.8: Estimated probability of bending versus crushing failure as a function of ice thickness. (Hendrikse, 2024)

4.3. Svea Case Study

4.3.1. Ice Conditions

Field measurements at Svea were carried out between 26 and 28 March 2025. The work was conducted near the former mining settlement of Sveagruva by students from UNIS as part of their AT311-Sea Ice Mechanics course. At Svea, the average daily air temperature in December remained around -5°C, with some days rising just below freezing, as shown in Figure 4.1. Two warm periods occurred in early and late February, where average temperatures exceeded 0°C. A cold period in late March was observed

two weeks prior to the testing which brought temperatures down to around -20°C. During the testing period itself, the average air temperature was approximately -10°C, with cloud conditions changing between overcast and partly clear. A light snowfall occurred on the 27th of March and approximately 5 cm of fresh snow was present the following day. The ice cover was continuous with a thickness between 58 and 68 cm across the test area. Snow thickness ranged from 22 to 34 cm. All BHJ tests were performed within a 50x50 m area on stable, undisturbed ice.

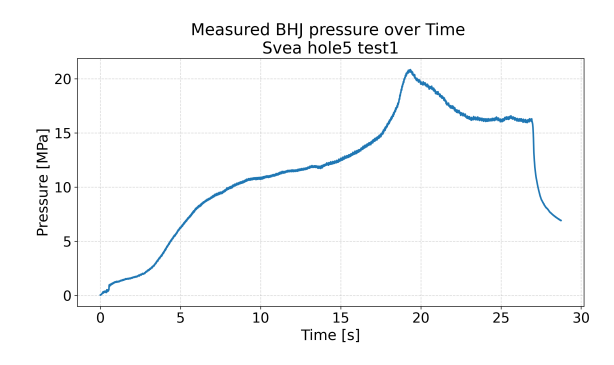
4.3.2. BHJ Strength Measurements

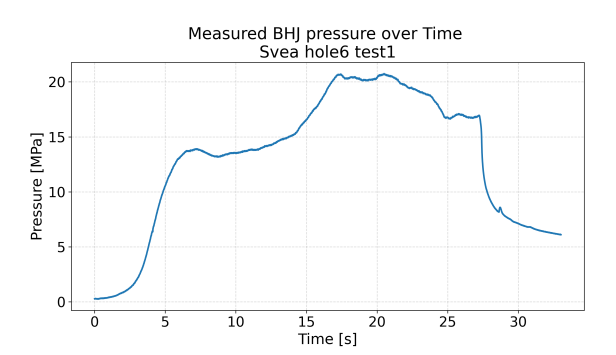
A total of nine boreholes were tested at the Svea field site, with two BHJ measurements performed in each hole. This resulted in 18 measurements of confined compressive strength. The results after multiplication by the calibration factor of 2.13 are shown in Table 4.5.

Table 4.5: Maximum measured BHJ pressure for the two tests performed in each hole at Svea. Tests were carried out between 26 and 28 March 2025.

Hole	Test 1 [MPa]	Test 2 [MPa]
1	13.20	15.74
2	16.62	18.78
3	14.04	14.94
4	16.18	19.12
5	20.84	14.35
6	20.75	17.19
7	16.63	16.14
8	16.54	14.88
9	13.29	15.26

The measured strength values ranged from 13.20 MPa to 20.84 MPa. The average strength index, $\sigma_{\text{BHJ},0}$, across all tests was 16.36 \pm 2.25 MPa. These values are approximately 75% higher than those recorded at Hjellbotn. Figure 4.9 presents the two highest BHJ pressure curves from the Svea case study. The remaining pressure graphs are shown in Appendix A.2.





(a) BHJ test in Hole 5, Test 1. The pressure curve shows a wavy increase over the first 18 seconds. A maximum pressure of 20.84 MPa is reached just before a sudden drop, followed by a steady plateau.

(b) BHJ test in Hole 6, Test 1. The pressure shows a steep wavy increase, reaching a plateau at 20.75 MPa between 16–21 seconds. After this plateau, the pressure gradually decreases.

Figure 4.9: Borehole Jack pressure over time curves from Hole 5 and Hole 6 at Svea.

4.3.3. Temperature Profile

The ice temperature was measured by inserting a probe at regular intervals of approximately 4-5 cm along the length of extracted cores. Each core was tested immediately after retrieval to minimize the thermal disturbance. The complete vertical profile is shown in Figure 4.10. The recorded temperature values show a steady increase from the top towards the bottom of the ice, ranging from -4.45 $^{\circ}$ C near the surface to -1.94 $^{\circ}$ C at the ice-water interface. This gradient indicates the internal heat transfer and the insulating effect of the snow cover. The bottom temperature approaches the freezing point of the

4.3. Svea Case Study

39

sea water.

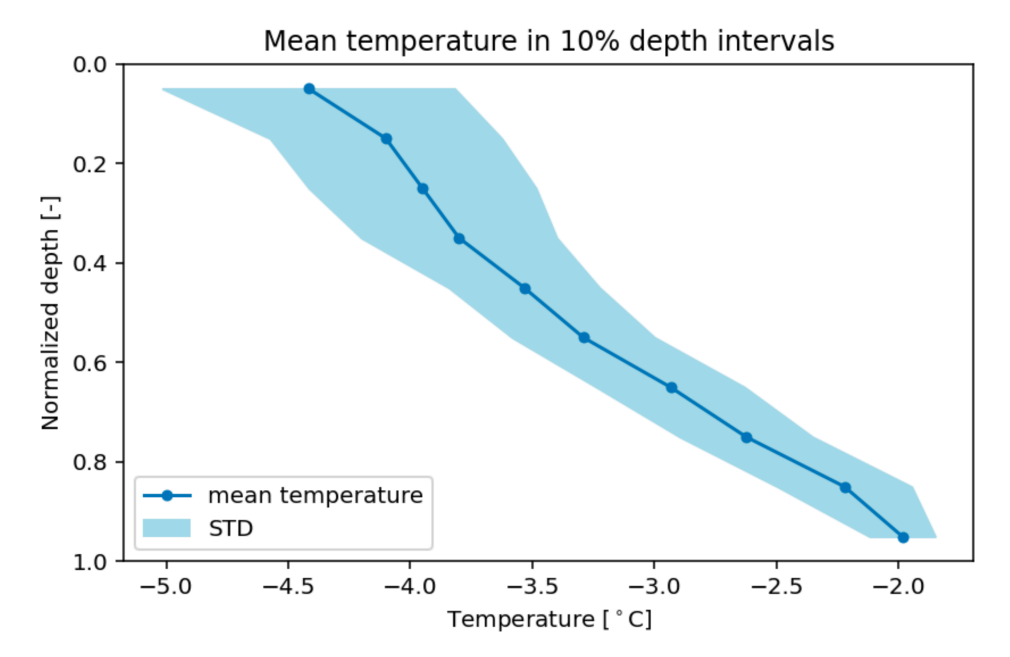


Figure 4.10: Vertical ice temperature profile from Svea. Values represent the average of 10 layers over the normalized depth. Graph obtained from course report: (UNIS, 2025).

4.3.4. Salinity Profile at Svea

Salinity values were obtained from melted ice core segments retrieved from the ice column. The average salinity profile shows a C-shape, with the highest concentrations at the top and bottom layers and a minimum near the center. The average salinity values across the ice thickness ranged from 4.1 to 9.3 ppt. This means the ice near Svea had over 20 times more salt than the ice at Hjellbotn. The top layer showed the greatest variability across cores, while bottom layer values were more consistent. This is likely due to less environmental disturbance. The mean salinity over depth is shown in Figure 4.11.

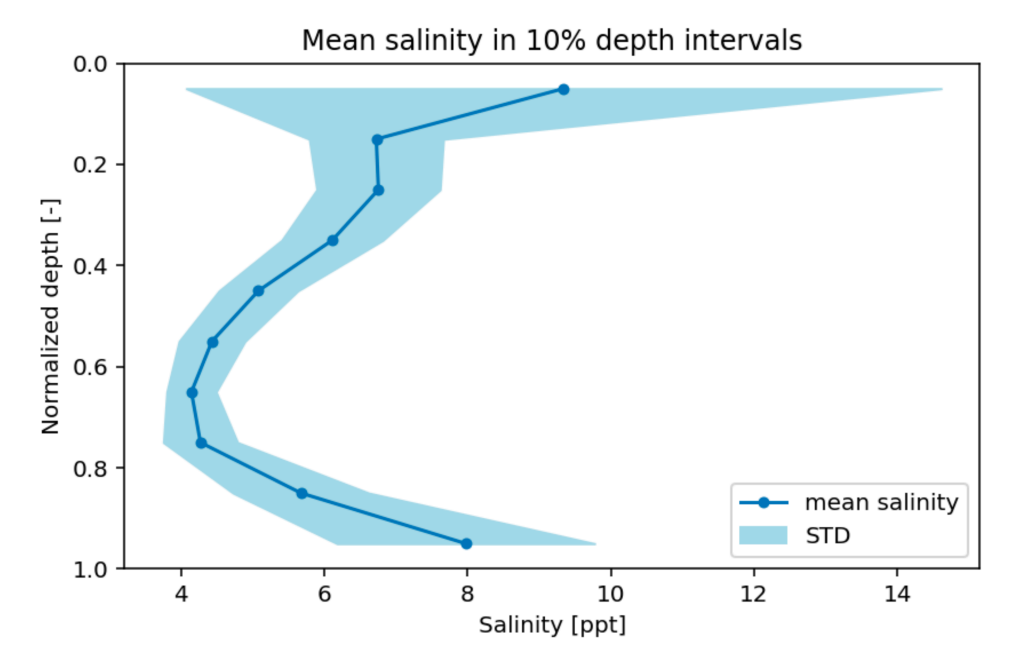


Figure 4.11: Average vertical salinity profile at Svea. A C-shaped curve is visible, with peak values near the ice surface and bottom. Graph obtained from course report: (UNIS, 2025).

4.3.5. Density Profile at Svea

Ice density was measured at Svea using the hydrostatic method. Measurements were done at nine vertical cores from top to bottom, spaced evenly across the ice thickness. The full density profile is shown in Figure 4.12. The density values ranged from 855 kg/m³ at the surface to 920 kg/m³ at the bottom. The largest change was observed in the top 20% of the core, where the density increased rapidly from 855 to 895 kg/m³. Likely due to a refrozen snow layer, which results in a lower density. Below this point, the density profile stabilized, with only small increases over the remaining depth.

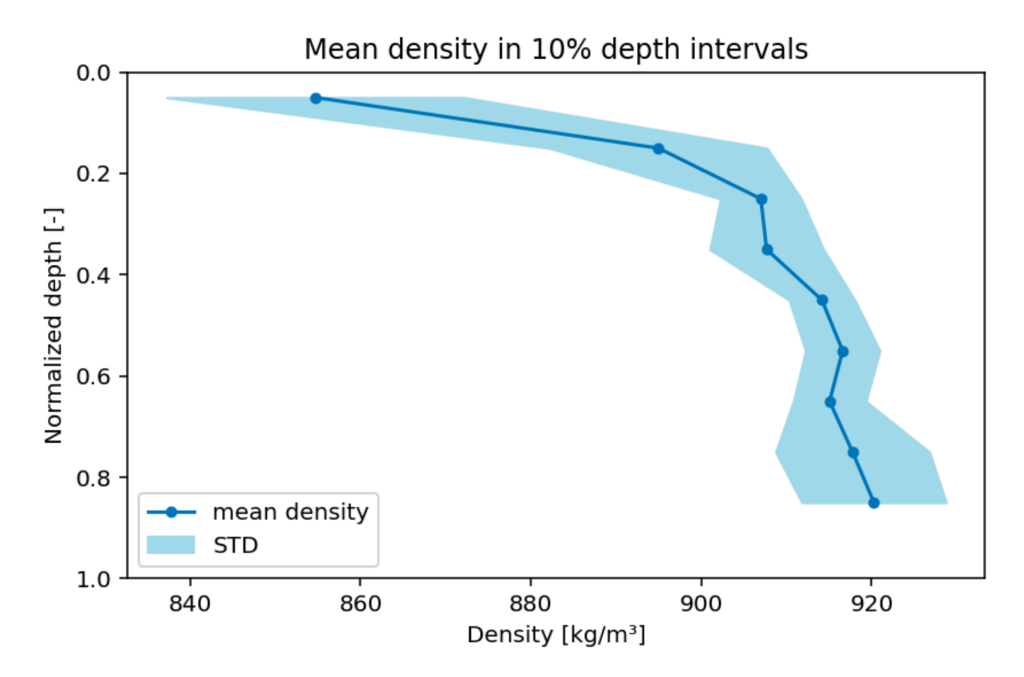


Figure 4.12: Vertical density profile from a representative ice core at Svea. A rapid increase is seen in the upper part of the ice. Graph obtained from course report: (UNIS, 2025).

4.3.6. Interpretation of Test Results at Svea

The BHJ strength measurements at Svea ranged between 13.20 and 20.84 MPa, with an average value of 16.36 ± 2.25 MPa. During these measurements, no spalling was observed. All tests were carried out within a confined area of approximately 50 by 50 m. While the spatial variability of the ice sheet was not explicitly studied, the extent of the sampled area introduces uncertainty regarding the representativeness of the region. Local variations outside this area may exist which could lead to higher or lower strength values.

Similar to Hjellbotn, BHJ measurements at Svea were performed at half the ice thickness. However, since the ice at Svea exhibited a relatively uniform structure, the likelihood of missing significantly stronger layers during the BHJ measurements is reduced. Large differences in mechanical strength are therefore probably limited along the different layers, except close to the edges of the ice sheet, where confinement effects become more relevant.

Salinity values measured at Svea ranged from approximately 4 to 8 ppt, slightly lower than typical first-year sea ice which can be around 10 ppt. The lower salinity and homogeneous structure suggest that the ice formed under relatively stable thermodynamic conditions. The coring process itself may have introduced slight uncertainties in density and salinity measurements due to brine drainage during core extraction. Near the ice surface, variable snow depths resulted in differences in ice insulation. This difference in insulation resulted in a temperature variation of up to 1.5°C. Such insulation effects could influence the mechanical properties and the estimation of brine volume.

4.4. Case Study Comparison

This section presents the main results of the processed data from both locations. It compares the strength indices obtained from both methods and looks at the factors influencing the indices. The strength indices are then used to obtain a Reduction factor and corresponding value for $C_{\rm R,s}$.

4.4.1. Sensitivity of Brine Volume to Temperature

The accuracy of the temperature sensor used for the case study was $\pm~0.3^{\circ}\text{C}$. To understand the impact of this measurement uncertainty, a sensitivity study was performed. This evaluates how small temperature measurement variations affect the computed brine volume, depending on the method used. This is important because the final ice strength index is directly influenced by the calculated brine volume. The methods used for this study are the UNESCO equilibrium method, used for warm brackish ice at Hjellbotn, and the Frankenstein method, used for colder sea ice at Svea. Both are detailed in Section 2.4.1. At Hjellbotn, the average salinity was measured as 0.16 $\pm~0.05$ ppt. For Svea, the average salinity was 5.73 $\pm~1.2$ ppt. The ice temperatures were around -0.2°C for Hjellbotn and -3.5°C for Svea.

The results for the sensitivity analysis at Hjellbotn are shown in Table 4.6. At these warm temperatures, the brine volume changes rapidly with temperature. A change from -0.2°C to -0.1°C more than doubles the estimated brine volume. The ISO based values are in general lower than the UNESCO values, with differences of around 9% at -0.5°C, increasing to 15% at -0.05°C.

Table 4.6: Calculated brine volume using the ISO A.6-6 and UNESCO method over different temperature values with a fixed salinity of 0.16 ppt.

T_{ice} [°C]	v_b (ISO A.6-6)	v_b (UNESCO)
-0.50	0.015	0.017
-0.40	0.019	0.022
-0.30	0.026	0.029
-0.20	0.038	0.044
-0.10	0.077	0.089
-0.05	0.154	0.178

For Svea, Table 4.7 shows that the effect of temperature variation is smaller. The 0.3° C accuracy range of the thermometer causes less than 10% change in brine volume. The ISO and Frankenstein methods give similar results, with the Frankenstein method estimating the brine volume approximately 5% lower. The values include the correction factor of 0.98 from Equation (2.13) to account for the local ice density at Svea of 900 kg/m³.

Table 4.7: Brine volume calculated using the ISO A.6-6 and UNESCO method over different temperature values with a fixed salinity of 5.73 ppt.

T_{ice} [°C]	v_b (ISO A.6-6)	v_b (UNESCO)
-3.8	0.075	0.071
-3.7	0.077	0.072
-3.6	0.079	0.074
-3.5	0.082	0.076
-3.4	0.084	0.079
-3.3	0.086	0.081

The results from both tables indicate that the brine volume in warm ice is more sensitive to small changes in temperature. At Hjellbotn, a 0.1° C shift can change the volume by over 30%. At Svea, the same temperature change results in a much smaller change of less than 5%. This sensitivity is important because the ice temperature measurement accuracy was \pm 0.3°C, which introduces large uncertainty in the brine volume. The effect of temperature change becomes more significant when the

brine volumes are converted to strength indices, σ_{Bri} , using the ISO strength-brine relationship. This will be further discussed in Section 4.4.2.

4.4.2. Strength Index Values

This subsection provides an overview of the strength index values used in this study. For the BHJ method, only tests without visible spalling were included. This improves consistency with the Svea site, where no spalling was observed. At Hjellbotn, the resulting BHJ strength index was $\sigma_{\text{BHJ},s}$ = 9.33 \pm 2.25 MPa. The ice thickness was 12-14 cm and the average temperature was -0.2°C. For Svea, the BHJ strength index was $\sigma_{\text{BHJ},0}$ = 16.31 \pm 2.25 MPa, with ice thickness 58-68 cm and temperature -3.46 \pm 0.90°C. This indicates that Svea ice was approximately 75% stronger than that at Hjellbotn, based on BHJ measurements.

Table 4.8: Overview of ice strength index values from BHJ tests at Hjellbotn (specific area of interest) and Svea (reference area).

Area	Origin	Symbol	Value [MPa]
Specific area of interest	Measured, Hjellbotn	$\sigma_{ m BHJ,s}$ $\sigma_{ m BHJ,0}$	9.33 ± 2.25
Reference area	Measured, Svea		16.31 ± 2.25

For the brine volume method, the UNESCO equation and ISO Equation A.6-6 were used for the brackish warm Hjellbotn ice. The results are presented in Table 4.9. The UNESCO-based strength index was approximately 10% lower than Equation A.6-6 proposed in ISO 19906. For Svea, the ISO method and the Frankenstein method gave nearly identical results. This suggests that the generalized equation used in ISO is valid for cold ice. The ISO reference strength index, $\sigma_{\text{Bri},A,0}$, does not include a stated error, so a 5% uncertainty was assumed to match other standard errors.

Table 4.9: Summary of ice strength index values $\sigma_{{\sf Bri},x}$, based on the brine volume method.

Area	Origin	Method	Symbol	Value [MPa]
Specific area of interest	Measured, Hjellbotn	UNESCO	$\sigma_{Bri,u,s}$	2.12 ± 0.13
	Measured, Hjellbotn	ISO (A.6-6)	$\sigma_{Bri,is,s}$	2.38 ± 0.16
Reference area	Measured, Svea	Frankenstein	$\sigma_{Bri,f,0}$	1.09 ± 0.09
	Measured, Svea	ISO (A.6-6)	$\sigma_{\sf Bri,is,0}$	1.08 ± 0.08
	Design Value	ISO Arctic reference	$\sigma_{ m Bri,A,0}$	2.86 ± 0.14 ^a

^a A standard error of 5% was applied to the ISO Arctic reference value (2.86 MPa) to reflect dataset variability and uncertainty.

Temperature Effect on $\sigma_{\rm Bri}$

To study how small changes in measured ice temperature influence the resulting strength index $\sigma_{\rm Bri}$, the sensitivity analysis from Section 4.4.1 was also conducted for the strength index based on brine volume. The analysis uses a constant salinity and varies the temperature across the accuracy range of the used thermometer. The resulting brine volumes were converted to strength values using ISO's brine-strength interpolation Figure 2.3. For Hjellbotn, the UNESCO and ISO methods were compared with a salinity of 0.16 ppt. The results are presented in Table 4.10. The table shows that when temperature increases from -0.5°C to -0.05°C, within the accuracy range of the thermometer, the predicted strength drops from 4.9 MPa to around 0.85 MPa using the ISO method. The UNESCO method shows almost an identically large decrease. A change of 0.2-0.3°C can result in a strength difference of over 1 MPa. This indicates that at warm temperatures, small errors in temperature measurement can significantly impact the resulting ice strength index.

Temperature [°C] $\sigma_{\rm Bri,u,s}$ [MPa] $\sigma_{\text{Bri,is,s}}$ [MPa] 4.968 -0.504.588 -0.404.235 3.770 -0.30 3.295 2.991 -0.202.203 1.823 -0.101.161 1.057 -0.050.845 0.811

Table 4.10: Sensitivity of σ_{Bri} to temperature changes for warm ice at a fixed salinity of 0.16 ppt.

At Svea, where the salinity was around 5.73 ppt on average, the same analysis was done using both the ISO and Frankenstein methods. The results are shown in Table 4.11. Unlike at Hjellbotn, the strength values change little with temperature. Over the tested range, a 0.5°C change only changes the strength index by about 0.1 MPa. Also, the ISO and Frankenstein methods give nearly the same values, with a difference of less than 0.05 MPa. This confirms that for cold ice, the strength estimate is less sensitive to the temperature measurement uncertainty.

Table 4.11: Sensitivity of σ_{Bri} to temperature change in cold ice at a fixed salinity of 5.73 ppt.

Temperature [°C]	$\sigma_{\mathrm{Bri},\mathrm{is},\mathrm{0}}$ [MPa]	$\sigma_{\mathrm{Bri},\mathrm{f},\mathrm{0}}$ [MPa]
-3.80	1.180	1.230
-3.70	1.159	1.218
-3.60	1.138	1.194
-3.50	1.117	1.172
-3.40	1.096	1.141
-3.30	1.077	1.122

The results indicate that the temperature effect is much more critical in warm brackish ice like Hjellbotn. A small error in temperature can shift the predicted strength by several MPa. In cold Arctic-like ice, as found at Svea, the temperature effect is more stable and less sensitive to the same change in temperature.

4.4.3. Reduction Factor

The reduction factor R is used to scale the ice strength coefficient C_R to a specific area of interest. It is calculated as the ratio between the local strength index, σ_s and a reference strength index, σ_0 , as described in Section 2.4.2. This section presents the results of the data processing used to calculate the reduction factor for both methods. The difference between the reduction factor obtained from the BHJ method and the Brine method is further discussed in Chapter 5.

Reduction Factor from BHJ Method

The BHJ strength indices were obtained from in-situ mechanical tests. Only the tests without visible spalling were included. The average strength index at Hjellbotn was $\sigma_{BHJ,s}$ = 9.33 \pm 2.25 MPa, while the Arctic reference value at Svea was $\sigma_{BHJ,0}$ = 16.31 \pm 2.25 MPa. This results in a reduction factor of:

$$R_{\rm BHJ} = \frac{\sigma_{\rm BHJ,s}}{\sigma_{\rm BHJ,0}} = \frac{9.33}{16.31} = 0.57 \pm 0.15$$

Using this reduction factor and the Arctic reference strength coefficient C_{R0} = 2.8 MPa, the scaled $C_{R,s}$ for the area of interest becomes:

$$C_{
m R,s} = R_{
m BHJ} \cdot C_{
m R0} = 0.57 \cdot 2.8 = 1.60 \, \pm 0.42 \
m MPa$$

This $C_{R,s}$ value suggests a strength lower than $C_R = 1.8 \,\text{MPa}$ for temperate regions. This aligns with expectations given Hjellbotn's geographical position and its limited FDD.

Reduction Factors from Brine Volume Method

The brine volume approach uses measured temperature and salinity to estimate the ice strength index, σ_{Bri} . Table 4.12 presents the calculated reduction factors based on these methods.

Table 4.12: Reduction factors based on the brine volume method. Each factor is defined as $R_{x,y} = (\sigma_{\text{Bri},x,s}/\sigma_{\text{Bri},y,0})$, where x denotes the method used for the specific area of interest and y the method or reference value used for the reference area.

Reduction Factor	Value
$\begin{array}{c} R_{\rm is,f} = (\sigma_{\rm Bri,is,s}/\sigma_{\rm Bri,f,0}) \\ R_{\rm is,is} = (\sigma_{\rm Bri,is,s}/\sigma_{\rm Bri,is,0}) \\ R_{\rm is,A} = (\sigma_{\rm Bri,is,s}/\sigma_{\rm Bri,A,0}) \end{array}$	2.20 ± 0.26 2.20 ± 0.25 0.83 ± 0.10
$\begin{array}{c} R_{\rm u,f} = (\sigma_{\rm Bri,u,s}/\sigma_{\rm Bri,f,0}) \\ R_{\rm u,is} = (\sigma_{\rm Bri,u,s}/\sigma_{\rm Bri,is,0}) \\ R_{\rm u,A} = (\sigma_{\rm Bri,u,s}/\sigma_{\rm Bri,A,0}) \end{array}$	1.94 ± 0.22 1.96 ± 0.22 0.74 ± 0.09

For Hjellbotn, the difference between using the UNESCO method and the ISO method was approximately 10%. At Svea, the Frankenstein and ISO equations gave nearly identical results. This was expected given the similar structure of the formulas. Both $R_{\rm is,A}$ and $R_{\rm u,A}$ indicate that the ice at Hjellbotn is approximately 0.79 \pm 0.09 times weaker than the ISO Arctic reference. This reduction is in line with ISO's guidance to reduce $C_{\rm R}$ for regions with fewer freezing degree days.

Effect of Temperature on Reduction Factor

Brine-based strength index is sensitive to small temperature changes in warm ice near 0° C. Table 4.13 shows how reduction factor $R_{is,A}$ and the resulting $C_{R,s}$ change for a small range of temperatures.

Table 4.13: Change in $R_{\rm is,A}$ and corresponding scaled ice strength coefficient $C_{\rm R,s}$ with temperature at Hjellbotn. Values are calculated using the ISO Arctic reference strength $\sigma_{\rm Bri,A,0}=2.86$ MPa and a fixed salinity of 0.16 ppt.

Temperature [°C]	$R_{\rm is,A}[-]$	$C_{R,s}$ [MPa]
-0.40	1.48	4.14
-0.35	1.32	3.68
-0.30	1.15	3.22
-0.20	0.77	2.16
-0.10	0.41	1.15
-0.05	0.30	0.84

A 0.3° C drop in ice temperature, from -0.2° C to -0.5° C, increases the reduction factor from 0.77 to 1.74. This nearly triples the scaled strength coefficient. These temperature variations fall within the error margin of the sensor used in the field. This indicates that for warm ice, temperature measurement accuracy is crucial and results should be interpreted with care. For Svea, with ice temperatures around -3.5° C, a similar sensitivity analysis showed less than 5% variation in R and corresponding $C_{R,s}$. This confirms that temperature variations have a minimal influence on strength calculations for colder ice.

5

Discussion

ISO 19906 suggests that the ice strength coefficient C_{R} can be scaled between sites by comparing the compressive strength of the ice. It also assumes that the reduction factor between two sites should be the same for different strength estimation methods. Provided that the same method is used at both the reference site and the site of interest. This assumption is tested in this work.

Two strength estimation methods were used. Both methods were applied at Svea and Hjellboth during the field campaigns. These methods are measuring different aspects of ice strength. The BHJ test captures structural strength and fracture resistance of the in-situ ice, including effects of ice texture, pre existing cracks and confinement. On the other hand, the brine volume method predicts the intrinsic material compressive strength based on temperature and salinity.

5.1. Reduction Factor: Svea vs. Hjellbotn

ISO 19906 proposes that the ice strength coefficient $C_{\rm R}$ can be scaled to a specific site by comparing a local strength index $\sigma_{\rm S}$ with a reference strength index $\sigma_{\rm O}$. The resulting reduction factor $R=\sigma_{\rm S}/\sigma_{\rm O}$ is used to compute a site-specific $C_{\rm R}$.

Two different methods to obtain σ were used in this study: the borehole jack (BHJ) method and the brine volume method. The BHJ method gives in-situ compressive strength, while the brine volume method estimates ice strength using temperature and salinity input. For cold ice, the Frankenstein model was used. For warm, brackish ice, the UNESCO method was used. These models were selected as they are suitable for the specific temperature regimes of Svea and Hjellbotn.

Observed Reduction Factors and Implications

The observed reduction factors were derived from both BHJ and brine volume-based methods. At Svea, the BHJ method showed higher compressive strength compared to Hjellbotn, which resulted in a reduction factor of $R_{\rm BHJ}$ = 0.57 \pm 0.15. This suggests a 43% lower strength at Hjellbotn relative to the Arctic reference. The brine volume method at Hjellbotn, using the UNESCO standard, resulted in a lower strength than the ISO Arctic reference value. This resulted in a reduction factor of $R_{\rm Bri,u,A}$ = 0.74 \pm 0.09. When instead using the locally measured strength at Svea as the reference value for the arctic, the reduction factor increased significantly to $R_{\rm Bri,u,f}$ = 1.94 \pm 0.22 , which implies a considerably stronger ice at Hjellbotn than expected. The corresponding site-specific strength coefficients were calculated using Equation (2.15). The results are summarized in Table 5.1.

 $C_{\mathsf{R},\mathsf{s}}$ [MPa] **Reduction Method** $\sigma_{\rm s}$ [MPa] σ_0 [MPa] R [-] 9.33 ± 2.25 0.57 ± 0.15 1.60 ± 0.42 BHJ-based (R_{BHJ}) 16.31 ± 2.25 Brine, UNESCO & Arctic ($R_{Bri,u,A}$) 2.12 ± 0.13 2.86 ± 0.14 0.74 ± 0.09 2.07 ± 0.25 Brine, UNESCO & Frankenstein ($R_{Bri.u.f}$) 2.12 ± 0.13 1.09 ± 0.09 1.94 ± 0.22 5.43 ± 0.62

Table 5.1: Comparison of strength estimates and reduction factors using BHJ and brine methods.

The BHJ-based $C_{\rm R}$ = 1.60 MPa and the brine-based $C_{\rm R}$ = 2.07 MPa (using the ISO Arctic reference value) are reasonably close. This supports the idea that both approaches can give reasonable estimate of the regional strength when a correct reference value is used. However, using the local Svea brine strength as a reference results in a much higher $C_{\rm R}$ = 5.43 MPa, which also indicates a higher ice strength at Hjellbotn. This seems rather unrealistic, given the suggestion ISO recommendation to reduce ice strength in areas with lower FDD (ISO19906, 2019; Paquette & Brown, 2017). For instance, ISO recommends a strength coefficient of 1.8 MPa for temperate ice regions, which suggests that Hjellbotn ice, being thin, brackish with and formed under even fewer FDD, should also have a lower ice strength.

It is understood that warm ice has lower strength, while freshwater ice tends to be stronger. However, the mechanical behaviour of warm brackish ice is less well defined. In this study, the brine volume method indicated a high strength for Hjellbotn ice. Whether this value reflects the actual strength of the ice remains uncertain, as the brine method is an indirect measure and does not account for all physical characteristics such as porosity or structural layering. These findings demonstrate that comparisons between sites are highly sensitive to the choice of reference value. When the local brine-based strength at Svea is used as the baseline, it leads to a high estimated strength for the ice at Hjellbotn. In contrast, applying ISO's Arctic reference strength produces a more moderate and consistent result, which aligns more closely with engineering expectations and observed BHJ results.

5.2. Influence of Ice Conditions on Measured Strength

The differences between the two methods can be partly explained by site-specific ice conditions and by what each method measures. Several factors likely contributed to the lower measured BHJ strength of Hjellbotn's ice, despite high brine-based strength estimates. The influence of ice thickness and confinement during testing, tidal movements and grounding, and differences between layered snow ice and columnar sea ice is discussed below.

5.2.1. Ice Thickness and Test Confinement

An important difference between the sites was the ice thickness. Svea's ice cover during the tests was about 58-68 cm thick, while the ice at Hjellbotn was much thinner, around 14 cm on average. The BHJ test results can be strongly influenced by ice thickness because of the degree of confinement the ice has during the test. In a thicker ice sheet, the surrounding ice provides more confinement when the jack applies pressure, allowing higher stresses to build up before failure. In very thin ice, however, stress from the jack can more easily cause fractures or flexural failure, resulting in a lower maximum pressure. This effect was visible in the results at Hjellbotn. BHJ tests where spalling occurred showed about 30% lower strength on average than tests without visible spalling. However, even tests without visible spalling may have been affected by reduced confinement. This likely contributed to the lower BHJ strength measured at Hjellbotn.

The influence of confinement across the ice sheet thickness can also be seen in the BHJ pressure-depth profile from Svea. As shown in Figure 5.1, the central ice layers, 25-35 cm depth, result in the highest strengths, suggesting a higher confinement. In contrast, both the uppermost and bottom layers show markedly lower strengths, consistent with weaker confinement near the boundaries. This illustrates how internal confinement varies across the ice thickness and directly affects measured strength. Influence from the snow layer on top resulting in weaker ice also plays a role in this effect. The ISO brine method, on the other hand, purely calculates strength from temperature and salinity; it has no parameter for ice thickness. Thus, it would not reflect this thickness effect. So, if one were to extrapolate $C_{\rm R}$ for very thin ice, relying solely on the brine derived strength may lead to problems. Without accounting for ice

thickness, such an approach may be non-conservative or misleading.

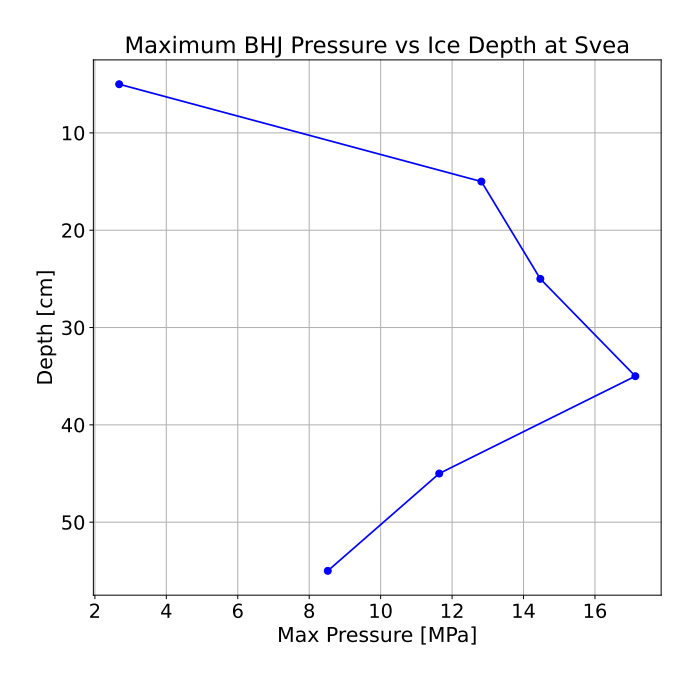


Figure 5.1: Maximum BHJ pressure measured at a depth interval of 10 cm in the 60 cm thick ice sheet at Svea. The plot shows how strength varies with depth, showing a peak in the middle layers with the top and bottom layers significantly weaker.

5.2.2. Tidal Movements and Grounding Effects

Hjellbotn's environment is a tidal fjord where the ice cover experiences daily vertical motions and grounding close to the shore during low tides. Such cyclical flexing introduces cracks and might weaken the ice sheet. Field observations noted that the ice in Hjellbotn was broken up prior to testing and had signs of stress from tidal movement, shown in Figure 4.2b. When the water level drops, the thin ice can settle and rests on the beach in shallow areas, then refloat with the rising tide. This process is repeatedly delaminating and fracturing the ice. This results in a reduction in the ice's ability to sustain load. The BHJ tests at Hjellbotn could have been influenced by this reduced ice strength. In contrast, the brine volume method would still compute strength based on the undamaged ice material properties because it assumes intact ice samples as taken from cores. As a result, any weakening due to macroscale cracking or cyclic damage would be missed. This explains part of why the brine method might overestimate the load-carrying strength of Hjellbotn's ice or, why the BHJ tests would underestimate the strength of the ice away from shallow areas.

5.2.3. Ice Composition and Density Differences

The ice composition at the two sites was notably different. Ice cores, density measurements and visual inspection showed that Hjellbotn's ice had a layered structure: a low-density, porous snow ice layer on top, with denser congelation ice below. This type of layering forms when surface snow melts or becomes flooded and then refreezes, creating a bubbly and relatively fresh upper layer. Snow ice contains more air and less salt than sea ice, this reduces both its density and reduces mechanical strength. In the Hjellbotn ice cores, the upper 3-5 cm had significantly lower density than the 10 cm ice beneath. In contrast, Svea's ice was more homogeneous. Its density remained stable between 900 and 920 kg/m³ over most of the thickness. Only the top 5-10% showed a slightly lower value around 855 kg/m³, likely from snow influence.

These differences in density and structure can explain some of the mechanical results. Hjellbotn's weak upper layer would reduce the load-bearing capacity of the ice sheet. The timing and weather conditions during the test campaign likely influenced the results as well. At Hjellbotn, the testing period followed snowfall, rainfall, and warm temperatures. These conditions caused surface melting and introduced inhomogeneity in the ice. This resulted in a layered structure with reduced strength. The brine volume

method indicated a high strength index for Hjellbotn ice ($\sigma_{Bri,u,s}$ = 2.12 \pm 0.13 MPa vs $\sigma_{Bri,f,0}$ = 1.09 \pm 0.09 MPa). This is because the lower salinity of the snow ice reduces the brine volume. However, this method does not account for mechanical weakness due to porosity or layering. As such, brine-based strength estimates may overpredict strength in complex or layered ice types. If temperatures had remained low before testing, the ice at Hjellbotn might have developed into a uniform 15-20 cm layer of congelation ice, observed in previous years (Høyland et al., 2025). Such a structure would have provided better confinement and likely resulted in higher BHJ strength. Ice strength in shallow fjords can vary significantly depending on weather and ice formation conditions. Thus, relying on one moment in the season may give non-representative results.

5.3. Temperature Sensitivity in the Brine Volume Estimation

The sensitivity study presented in Section 4.4 shows that the ice strength index $\sigma_{\rm Bri}$ and resulting reduction factor R are highly sensitive to small changes in ice temperature close to 0°C, Relevant for our area of interest, Hjellbotn, where the measured ice temperature was around -0.2°C and salinity was low (0.16 ppt). In this temperate range, the brine volume decreases rapidly with rising temperature. The conversion from brine volume to strength index $\sigma_{\rm Bri}$ makes this effect even stronger.

The thermometer used during both case studies had an accuracy of \pm 0.3°C. This full range leads to a difference in C_R of more than \pm 2.5 MPa. This corresponds to an increase of 125.5% in C_R when the temperature drops to -0.5°C, and an 61.1% decrease when the temperature rises from -0.2°C to -0.05°C.

The same sensitivity analysis for cold ice at Svea showed very small variation. Across the same temperature accuracy range around -3.5°C, the change in calculated brine volume and resulting $C_{\rm R}$ was around 5%. This shows that the temperature sensitivity of the brine-based strength estimation is mainly a concern for warm, low-salinity ice. These findings indicate that the uncertainty in the temperature measurement has a greater impact on the calculated strength and reduction factor than the choice of brine estimation method (Frankenstein/UNESCO vs. ISO A.6-6). It also indicates that for warm, brackish ice, the brine-based methods are unreliable. Therefore, in warm ice regions, the brine volume method should included with mechanical strength testing, such as BHJ or uniaxial compression tests to validate the results. The brine volume method alone, especially in near-freezing conditions, is insufficient to reliably estimate the ice strength coefficient $C_{\rm R}$ due to the high temperature sensitivity.

5.5. Limitations 49

5.4. Validity of the predefined Arctic ISO Reference value

The ISO 19906 standard suggests a reference strength index of $\sigma_{\text{Bri},\text{A},0}=2.86$ MPa for Arctic sea ice based on the brine volume method. This value is intended for use in regions with Arctic FY or MY ice. In this study, the same brine volume method applied to field data from Svea resulted in a much lower average strength of $\sigma_{\text{Bri},\text{f},0}=1.09\pm0.09$ MPa. This raises the question of whether Svea is a suitable proxy for Arctic conditions in the context of ISO 19906. Geographically, Svea lies in the Arctic region and the ice is saline. However, it should be noted that the ISO strength coefficient for the Arctic is primarily derived from full-scale structure-ice interactions in the Beaufort Sea. These Arctic ice conditions typically involve thicker, colder and more consolidated ice compared to what was observed at Svea. The number of Freezing Degree Days at Svea during the 2024/2025 winter was approximately 1050. In contrast, ISO suggests Arctic reference locations typically experience around 4000 FDD per winter season. The significantly lower FDD at Svea results in slower ice growth and higher average temperatures, both of which influence ice structure, properties and thus, ice strength.

The relatively low ice strength index based on brine volume at Svea may therefore be a result of these milder conditions. The FDD of 1050 falls within the range typically associated with Baltic sea ice conditions. However, Svea is not located in the Baltic region, and the ice was significantly more saline compared to this southern region. For this reason, Svea should not be classified as a Baltic reference site. An alternative classification may be sub-Arctic, which ISO 19906 associates with regions experiencing around 2000 FDD. While the FDD of Svea still falls below this threshold, it may share more characteristics with sub-Arctic than with fully developed Arctic ice. ISO 19906 does not provide a predefined brine-volume-based strength index for sub-Arctic conditions. This makes it difficult to validate or directly compare our own measurements.

The large difference in prescribed and actual FDD could explain the discrepancy between the measured strength index at Svea and the suggested predefined ISO reference strength index. For scaling purposes, using Svea as a proxy for the Arctic may introduce uncertainties in the estimation of $C_{\rm R}$. When the brine volume method is applied to such conditions, it may underestimate or overestimate the required strength adjustment when scaling towards other regions. Therefore, using a more accurate proxy region with thermal and structural characteristics closer to those described in the ISO standard, like the 4000 FDD, would likely improve the accuracy of the site-specific scaling method.

5.5. Limitations

During this study, several limitations influenced the interpretation of the results. Svea was used as a reference site for Arctic region due to its geographical position and accessibility, proximity to the University Centre in Svalbard (UNIS) within the available timeframe. However, the large differences in ice properties between Arctic sea ice and the brackish, temperate ice at Hjellbotn introduce scaling errors. The two sites differ not only in ice temperature and thickness, but also greatly in salinity, density, structure, and thus mechanical behaviour. These differences question whether scaling between such ice environments using the proposed scaling methods is appropriate, which is also explained in Section 2.4.3. A reference site with more similar properties compared to Hjellbotn, like one with fewer prescribed Freezing Degree Days and similar salinity might have provided a more consistent basis for scaling. For instance, a Baltic location could have resulted in more consistent results based on the brine volume method. However, such a comparison was not possible within the timeframe of this work and remains a topic for further investigation.

The timing of the field campaign may also limit the results. Although tests were done in at April, the ice may not have reached maximum strength. At Hjellbotn, brine may not have drained out yet, and the ice was still relatively warm. The maximum strength and seasonal effects like late winter consolidation, are then not fully captured (Timco & Johnston, 2002). This may have resulted in lower strength estimates compared to sampling later in the season.

For the BHJ testing at Hjellbotn, only tests without visible spalling were selected for analysis. This filtering process resulted in just four valid BHJ tests, which increases the overall uncertainty of the

5.5. Limitations 50

mechanical strength estimates. Moreover, the ice thickness at Hjellbotn was relatively low, and this may have affected the BHJ results. Thin ice can reduce lateral confinement, potentially leading to lower measured strengths. Currently, no minimum ice thickness or correction factor exists for valid BHJ testing in such conditions. It is also unclear whether this effect is specific to the BHJ method or if it reflects the actual mechanical behaviour of thin ice under structural loading. Therefore, the extent to which the reduced confinement in thin ice should influence the derived ice strength for design remains an open question. The field data in this study was collected from two single fjords. These may not fully represent broader regional ice conditions and spatial variability. However, if the single fjord is the specific area of interest for design purposes, does it qualify as a sufficiently large geographic area? There is a large room for interpretation here in the standard.

The brine volume method also has practical limitations. The temperature sensor used had an accuracy of $\pm~0.3\,^{\circ}$ C. For warm ice, like in Hjellbotn, small temperature changes lead to large changes in calculated strength. As shown in the sensitivity analysis, a temperature shift within the sensor's accuracy range can double the estimated strength. This makes the brine method unreliable when used alone in warm ice. At Hjellbotn, only two core samples were collected for brine volume and density analysis. These limited samples may not fully represent the site. Local variation in ice properties, especially near the coast, could influence the results. The area available for testing was small due to short daylight hours and safety limitations when working on the ice. The brine volume method itself is limited by its input parameters. It only uses salinity and temperature to estimate strength. Other factors like ice density, air content, porosity, and internal structure are not considered, even though they can significantly influence the true mechanical strength. This is particularly critical in layered or snow-influenced ice covers such as those found at Hjellbotn.

6

Conclusion

The aim of this work was to assess if local ice strength measurements from borehole jack tests and brine volume estimations can be used to derive a site-specific ice strength coefficient $C_{\rm R}$ from ISO 19906. Accurate estimation of $C_{\rm R}$ is important for the safe and cost-effective design of offshore wind structures in ice-affected waters. As the demand for offshore wind energy grows, ice-infested regions further south are becoming more attractive for development. However, limited data exist on how to accurately assess ice strength in such environments. This study evaluated the consistency, reliability, and practical limitations of two ISO-recommended approaches. It studied the direct approach of measuring the compressive strength using a BHJ. Next to this, the suggested indirect strength estimation based on brine volume, derived from ice temperature and salinity data was also studied.

To evaluate these methods, a case study with data from two locations was carried out. Hjellbotn near Trondheim was selected as a proxy location for future offshore wind turbines. It presented a more temperate site with brackish ice. Svea in the Svalbard archipelago represented Arctic ice conditions and served as a reference site. The results at Svea were obtained by the UNIS students of the course AT311 and the data was processed by the author. The ISO 19906 standard suggests two ice strength index reference values based on the Brine volume method, one for Arctic ice ($\sigma_{\rm Bri,A,0}$ = 2.86 MPa) and one for temperate regions ($\sigma_{\rm Bri,T,0}$ = 2,07 MPa). A site-specific ice strength coefficient $C_{\rm R}$ can be scaled from one of these predefined values. However, the standard does not give a reference strength value for BHJ measurements. This lack of guidance means that a representative Arctic strength value must be determined independently. In this study, Svea served as a proxy for the Arctic reference. Both BHJ measurements and salinity and temperature data for brine-based strength calculations were obtained. This was done to study the consistency between both methods.

The comparison between the two methods showed differences depending on the chosen reference value. The ratio between the strength index at the specific area of interest and a reference location is referred to as the reduction factor. It indicates how much the ice strength coefficient $C_{\rm R}$ from the reference location should be reduced or increased to obtain an appropriate $C_{\rm R}$ value for the specific area of interest. Based on BHJ testing, the reduction factor between Hjellbotn and Svea was: $R_{\rm BHJ}$ = 0.57 \pm 0.15. This results in a site-specific strength coefficient of $C_{\rm R}$ = 1.60 \pm 0.42 MPa. So the BHJ tests indicated a 43% reduction in strength at Hjellbotn compared to Svea. The brine volume method using the given Arctic ice strength index reference value, $\sigma_{\rm Bri,A,0}$, resulted in a higher reduction factor of $R_{\rm Bri,u,A}$ = 0.74 \pm 0.09. This reduction factor corresponds to a scaled $C_{\rm R}$ = 2.07 \pm 0.25 MPa. However, when the ice strength index obtained during the case study at Svea was used, the reduction factor increased to $R_{\rm Bri,u,f}$ = 1.94 \pm 0.22. Resulting in a much higher $C_{\rm R}$ = 5.43 \pm 0.62 MPa. This increase suggests that the warm and brackish ice at Hjellbotn is stronger than the Arctic ice. This overestimation indicates that the brine volume method might not be suitable for scaling the ice strength value $C_{\rm R}$ in these locations.

The study also revealed that the brine volume method is highly sensitive to small changes in temperature. At Hjellbotn, where the ice temperature was around -0.2°C, the thermometer used had an

accuracy of \pm 0.3°C. This uncertainty resulted in a variation of C_R between 0.84 MPa and 4.87 MPa. This is a strength increase of 125.5% when the temperature drops to -0.5°C, and a 61.1% decrease when it rises to -0.05°C. The conversion from brine volume to strength further amplifies these changes. For colder ice, such as at Svea, this sensitivity is much lower and the method remains more stable. While the BHJ method and brine method using the ISO reference value produced similar results, using local brine-derived references can lead to significant inconsistencies. This indicates that the assumption in ISO 19906, that different strength index estimation methods yield consistent reduction factors seems questionable. In locations like Hjellbotn, relying solely on the brine volume method can result in overestimated strengths, which could lead to unsafe design assumptions.

Because a newly developed jack was used in this study, a calibration study was carried out to increase the accuracy of the results during both case studies. The test rig applied loads similar to those recorded during fieldwork. Based on these tests, a calibration factor of c = 2.13 was found for air and ice temperatures between 0 and -5°C. This factor was used to convert the measured force from the jack into ice compressive strength.

In conclusion, the results show that while ISO 19906 provides a few steps to scale the value of $C_{\rm R}$, its application in warm or non-Arctic ice environments requires more consideration. The BHJ method and the brine volume method using the ISO Arctic reference value produced comparable reduction factors. However, when the brine-derived strength from our own Svea measurements was used as the reference, a high strength estimate for Hjellbotn was found. This indicated that it is important to chose the correct reference point for scaling the ice strength. A sensitivity analysis showed that the brine volume method is highly sensitive to small temperature changes near 0 °C, which can lead to large variations in strength estimates. These warm, brackish ice conditions are typical for potential offshore wind sites. Therefore, while the brine method may still be useful under such conditions, it is suggested that it be combined with direct strength measurements like the BHJ to ensure more reliable site-specific scaling for future offshore wind deployment.

Recommendations

This study presents a insight in comparing in-situ ice strength measurements across two areas using both mechanical testing and brine volume method. However, several improvements and extensions could improve the reliability of future research.

The number of BHJ tests conducted at each site was limited and the results could not be easily validated against other studies. Expanding the dataset would reduce uncertainty and improve confidence in the observed strength differences between regions. Currently, BHJ values mostly serve as an index. To make results more comparable across studies, a standardized method should be used. This requires a fixed indentation rate, geometry, and test guideline. A standard setup would enable consistent data collection and allow comparison of results across locations. Future studies should also perform BHJ testing alongside brine volume sampling. This would make it possible to evaluate how salinity and temperature influence the confined compressive strength measured by the jack. Repeating this combined testing throughout the ice season could provide insight into the relationship between ice property evolution and mechanical strength.

The brine based ice strength index could be expanded to include additional input parameters. Currently, only temperature and salinity are considered. Including measurements of porosity, density, or air content would improve estimates in complex or layered ice, such as snow-ice covers. Finally, more work is needed to assess the validity and applicability of the ISO 19906 reference values. Future studies should include Arctic or Temperate regions with well-developed ice, such as second-year or multi-year ice regions, to verify whether the ISO strength index $\sigma_{\text{Bri},A,0}$ and $\sigma_{\text{Bri},T,0}$ are representative. Including additional reference locations would support more accurate regional scaling of ice strength coefficients.

Bibliography

- Assur, A. (1960). Composition of sea ice and its tensile strength (Vol. 49). U.S. Army Snow, Ice; Permafrost Research Establishment, Corps of Engineers. https://catalog.hathitrust.org/Record/007266161
- Cox, G., & Weeks, W. (1982). Equations for determining the gas and brine volumes in sea ice samples. *Journal of Glaciology - GLACIOLOGY*, 29, 15. https://doi.org/10.1017/S0022143000008364
- Dempsey, J., Adamson, R., & Mulmule, S. (1999). Scale effects on the in-situ tensile strength and fracture of ice. part II: First-year sea ice at resolute, n.w.t. *International Journal of Fracture*, 95(1), 347–366. https://doi.org/10.1023/A:1018650303385
- Frankenstein, G., & Garner, R. (1967). Equations for determining the brine volume of sea ice from -0.5 to -22.9c. [Edition: 2017/01/30 Publisher: Cambridge University Press]. *Journal of Glaciology*, 6(48), 943–944. https://doi.org/10.3189/S0022143000020244
- Goldstein, R. V., & Osipenko, N. M. (2015). Some aspects of strength in sea ice mechanics. *Physical Mesomechanics*, *18*(2), 139–148. https://doi.org/10.1134/S102995991502006X
- Gravesen, H., & Kärnä, T. (2009). Ice loads for offshore wind turbines in southern baltic sea.
- Hammer, T. (2024). Ice-induced vibrations of offshore wind turbines.
- Hendrikse, H. (2017). *Ice-induced vibrations of vertically sided offshore structures* [Doctoral dissertation].
- Hendrikse, H. (2024, April 4). Ice loads on structures [AT-311/811].
- Hendrikse, H., & Owen, C. (2023). Application of the suggested ice strength coefficients in ISO 19906 to intermittent crushing. POAC.
- Hole, W. (1978). Eight report of the join panel on oceanographic tables and standards (Vol. 28). UN-ESCO.
- Hornnes, V., Høyland, K. V., Nord, T., & John, J. (2023). The development of layers in an ice cover in a sub-arctic norwegian fjord.
- Hornnes, V., Salganik, E., & Høyland, K. V. (2024). Relationship of physical and mechanical properties of sea ice during the freeze-up season in nansen basin. *Cold Regions Science and Technology*, 229, 104353. https://doi.org/https://doi.org/10.1016/j.coldregions.2024.104353
- Høyland, K., Nord, T., Hendrikse, H., Tuhkuri, J., Polojärvi, A., Von Bock und Polach, R. U., Heinonen, J., Eik, K., Teigen, S., Serre, N., Schümann, B., Granlund, V., von Borstel, T., Reimer, N., Haase, A., & Sjöblom, A. (2023). Challenges with sea ice action on structures for offshore wind.
- Høyland, K. V. (2009). Ice thickness, growth and salinity in van mijenfjorden, svalbard, norway. *Polar Research*, *28*(3), 339–352. https://doi.org/10.3402/polar.v28i3.6141
- Høyland, K. V. (2024). Ice actions on structures TBA4260, 2024 with corrections.
- Høyland, K. V., Hornnes, V., Vetter, H. D., Duprat, B., Pliss, A., & Wilmink, M. (2025). Ice thickness formation and growth of fjord ice in hjellbotn in the trondheim fjord, norway.
- ISO19906. (2019). *Petroleum and natural gas industries arctic offshore structures*. International Standardization organization.
- Jones, S. J. (1982). The confined compressive strength of polycrystalline ice [Edition: 2017/01/20 Publisher: Cambridge University Press]. *Journal of Glaciology*, *28*(98), 171–178. https://doi.org/10. 3189/S0022143000011874
- Kamesaki, K. (1996). Ice force as a function of structural compliance.
- Khonsari, M. M., & Booser, E. R. (2008). Introduction to tribology. John Wiley & Sons, Ltd.
- Kvale, N., Kornelia, N., & Omdal, H. (2019). Calibration of borehole jack.
- Lemström, I., Polojärvi, A., & Tuhkuri, J. (2022). Model-scale tests on ice-structure interaction in shallow water: Global ice loads and the ice loading process. *Marine Structures*, *81*, 103106. https://doi.org/https://doi.org/10.1016/j.marstruc.2021.103106
- Leppäranta, M., & Manninen, T. (1988). *The brine and gas content of sea ice with attention to low salinities and high temperatures*. Finnish Institute of Marine Research. http://hdl.handle.net/1834/23905

Bibliography 55

Li, G., Jiao, Y., Chen, X., Zhao, Y., Li, R., Guo, D., Ge, L., Hou, Q., & Wang, Q. (2024). Investigation of the recent ice characteristics in the bohai sea in the winters of 2005–2022 using multi-source data. *Water*, *16*(2), 290. https://doi.org/10.3390/w16020290

- Liu, F., Wang, X., Sun, F., & Kleidon, A. (2023). Potential impact of global stilling on wind energy production in china. *Energy*, 263, 125727. https://doi.org/10.1016/j.energy.2022.125727
- Määttänen, M., & Kärnä, T. (2011). ISO 19906 ice crushing load design extension for narrow structures. Proceedings of the International Conference on Port and Ocean Engineering under Arctic Conditions, POAC, 2, 903–911.
- Masterson, D., & Graham, W. (1995). Development of the original ice borehole jack. *Canadian Journal of Civil Engineering*, 23, 186–192. https://doi.org/10.1139/l96-019
- Paquette, E., & Brown, T. G. (2017). Ice crushing forces on offshore structures: Global effective pressures and the ISO 19906 design equation. *Cold Regions Science and Technology*, *142*, 55–68. https://doi.org/10.1016/j.coldregions.2017.07.010
- Parliament, E. (2020). An EU strategy to harness the potential of offshore renewable energy for a climate neutral future. Retrieved September 12, 2024, from https://eur-lex.europa.eu/legal-content/EN/TXT/?uri=COM:2020:741:FIN&qid=1605792629666
- Pustogvar, A., & Kulyakhtin, A. (2016). Sea ice density measurements. methods and uncertainties. *Cold Regions Science and Technology*, *131*, 46–52. https://doi.org/https://doi.org/10.1016/j.coldregions.2016.09.001
- Samardžija, I. (2024). Probabilistic assessment of first-year ice ridge loads on offshore structures.
- Schwarz, J., & Jochmann, P. (2001). Ice force measurements within the LOLEIF-project. *Proceedings POAC'01*, 2, 669–680.
- Schwarz, J., & Weeks, W. F. (1977). Engineering properties of sea ice [Edition: 2017/01/30 Publisher: Cambridge University Press]. *Journal of Glaciology*, 19(81), 499–531. https://doi.org/10.3189/S0022143000029476
- Schwarz, J., & Jochmann, P. (2009). Ice forces affected by temperature and thickness of the ice.
- Shi, W. (2020). Offshore wind turbine-ice interactions. In W. Cui, S. Fu, & Z. Hu (Eds.), *Encyclopedia of ocean engineering* (pp. 1–13). Springer Singapore. https://doi.org/10.1007/978-981-10-6963-5_135-1
- Sinha, N. K. (1987). The borehole jack—is it a useful arctic tool? *Journal of Offshore Mechanics and Arctic Engineering*, 109(4), 391–397. https://doi.org/10.1115/1.3257037
- Sinha, N. K. (2011). Borehole indentor a tool for assessing in-situ bulk ice strength and micromechanics. *Cold Regions Science and Technology*, 69(1), 21–38. https://doi.org/https://doi.org/10.1016/j.coldregions.2011.07.009
- Sinha, N. K., Shkhinek, K., & Smirnov, V. (2012). On borehole indentor (BHI) measurements and analysis. *Cold Regions Science and Technology*, 76-77, 109–120. https://doi.org/https://doi.org/10.1016/j.coldregions.2012.01.009
- Stachowiak, G., & Batchelor, A. W. (2005). Engineering tribology (3rd). Butterworth-Heinemann.
- Teigen, S. H., Høyland, K. V., & Moslet, P. O. (2005). Thermal stresses in first-year sea ice. https://api.semanticscholar.org/CorpusID:130849345
- Thijssen, J., & Fuglem, M. (2015). *Methodology to evaluate sea ice loads for seasonal operations* (Vol. Volume 8: Ian Jordaan Honoring Symposium on Ice Engineering). https://doi.org/10.1115/OMAE2015-42194
- Thijssen, J., Fuglem, M., Richard, M., & King, T. (2014). Implementation of ISO 19906 for probabilistic assessment of global sea ice loads on offshore structures encountering first-year sea ice. 2014 Oceans St. John's, OCEANS 2014. https://doi.org/10.1109/OCEANS.2014.7003190
- Timco, G. W., & Johnston, M. (2002). Sea ice strength during the melt season. 2, 187–193.
- Timco, G. W., & Weeks, W. F. (2010). A review of the engineering properties of sea ice. *Cold Regions Science and Technology*, 60(2), 107–129. https://doi.org/https://doi.org/10.1016/j.coldregions. 2009.10.003
- UNIS. (2025). Course AT-311: Sea ice mechanics and physics.
- Weeks, W. F. (2010). On sea ice. University of Alaska Press.
- Wilmink, M. (2024). On thin ice: What influences ice actions and how can this be tested? NTNU. Trondheim, Norway.



Boreholejack Results

A.1. Hjellbotn

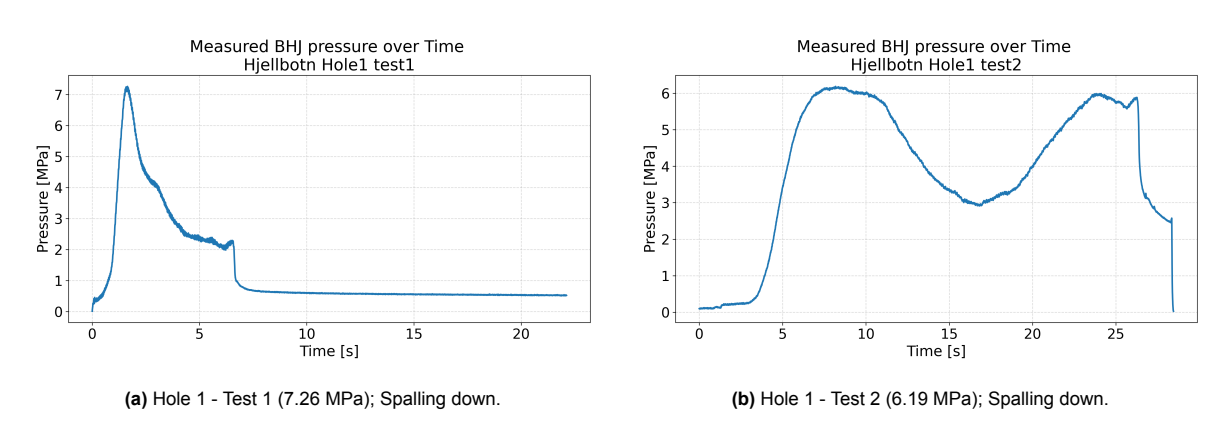


Figure A.1: Pressure vs Time plots for selected Hjellbotn BHJ tests, showing peak pressure and observed failure mode.

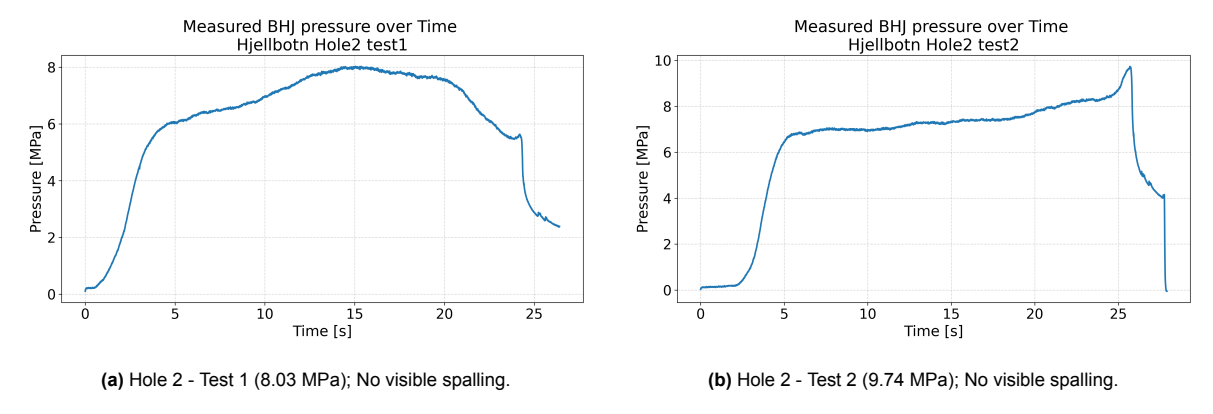


Figure A.2: Pressure vs Time plots for Hole 1 and Hole 2 tests at Hjellbotn.

A.1. Hjellbotn 57

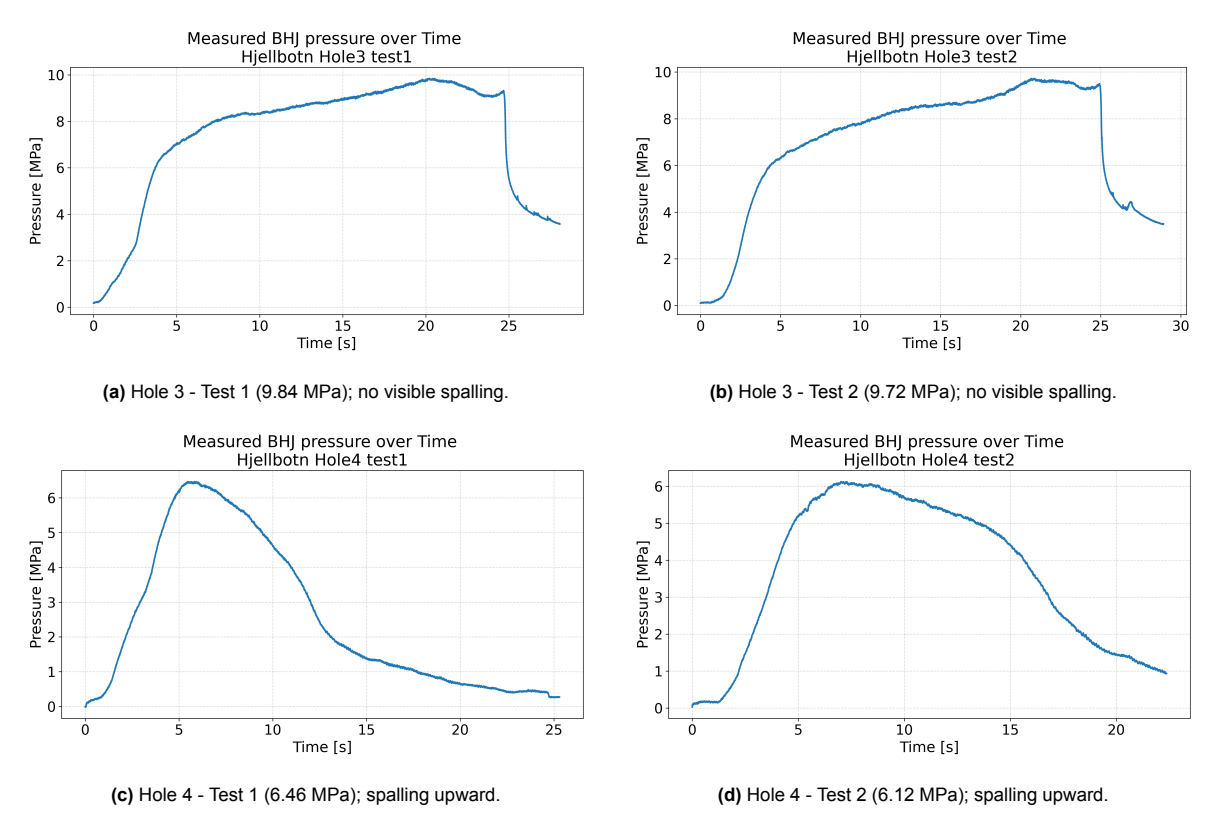


Figure A.3: Pressure vs Time plots for Hole 3 and Hole 4 tests at Hjellbotn.

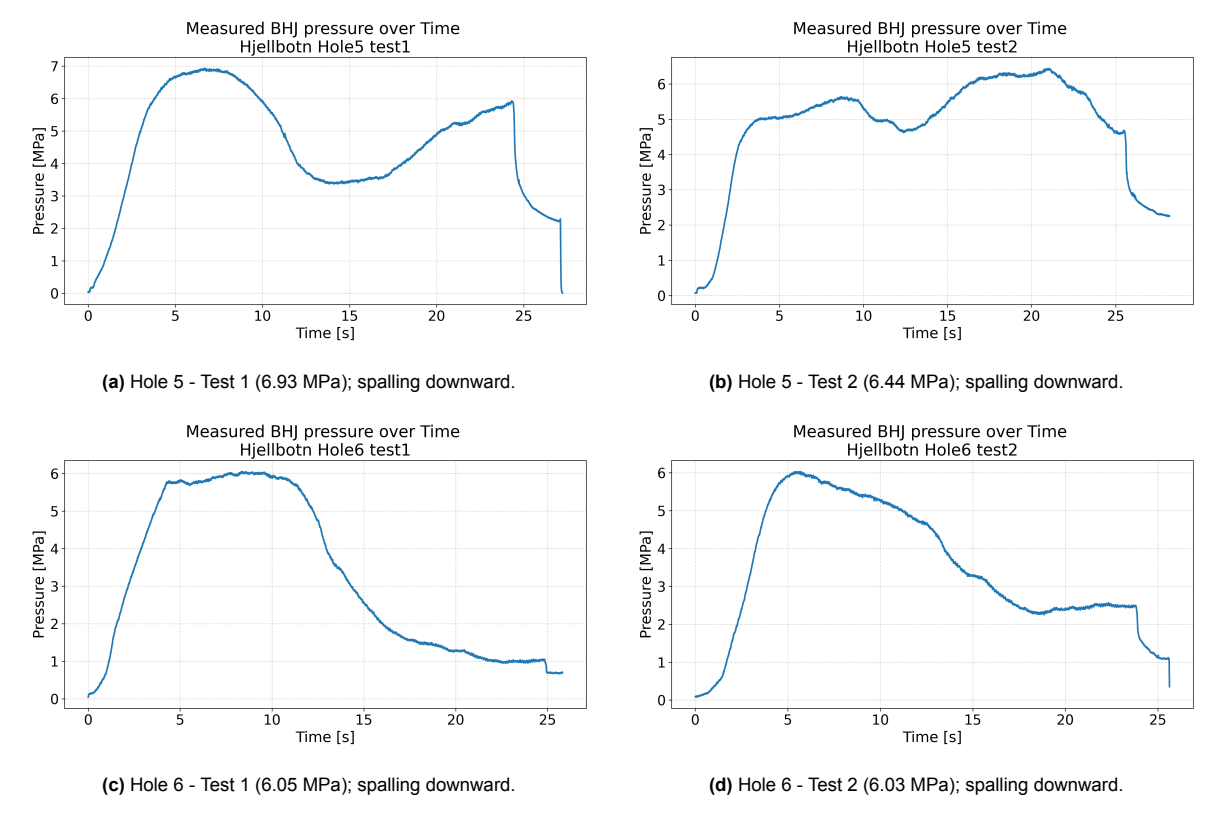


Figure A.4: Pressure vs Time plots for Hole 5 and Hole 6 tests at Hjellbotn.

A.2. Svea 58

A.2. Svea

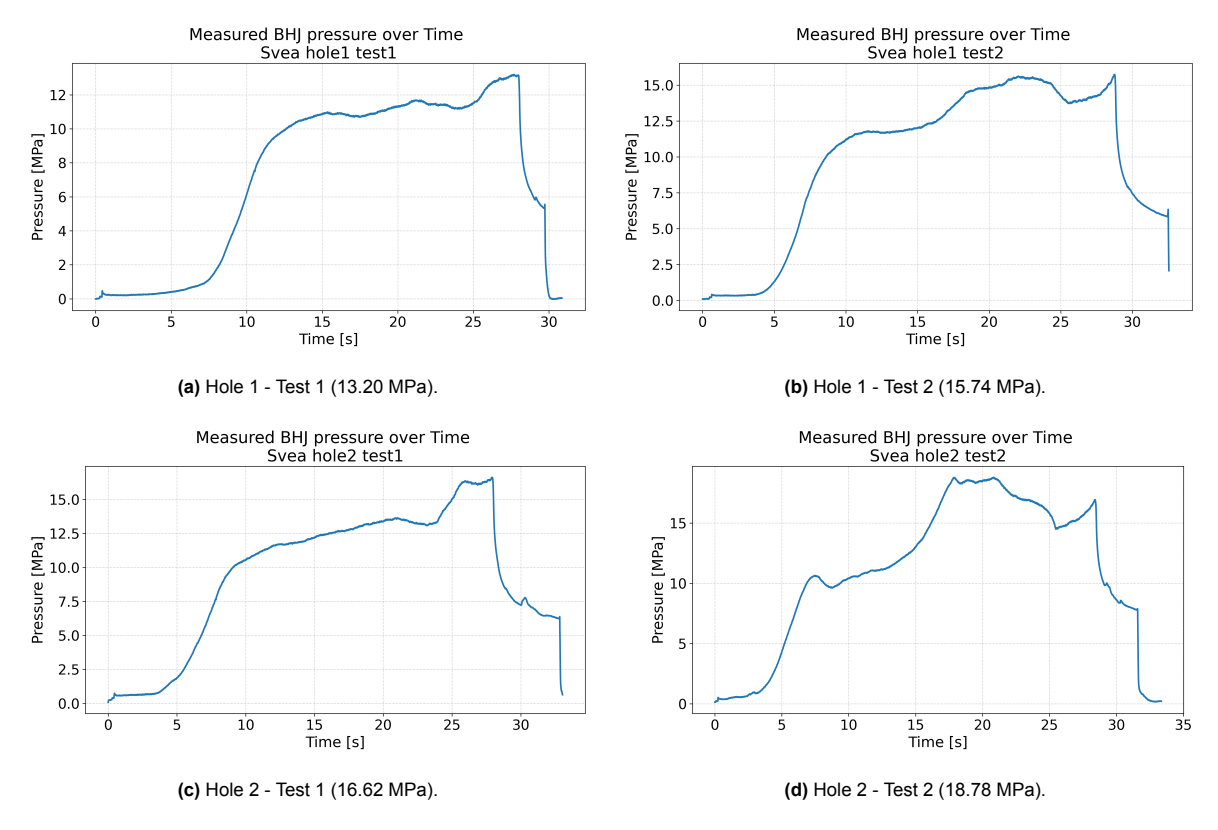


Figure A.5: Pressure vs Time plots for Hole 1 and Hole 2 at Svea.

A.2. Svea

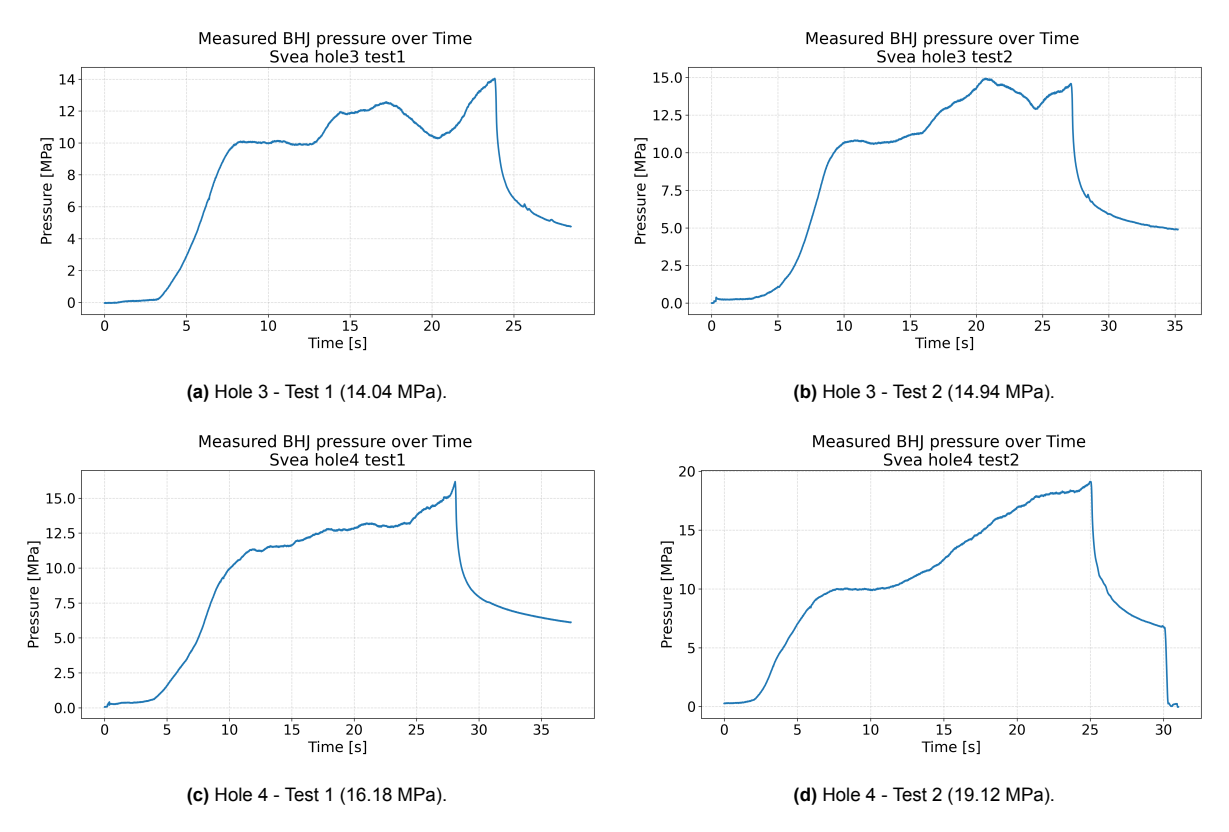


Figure A.6: Pressure vs Time plots for Hole 3 and Hole 4 at Svea.

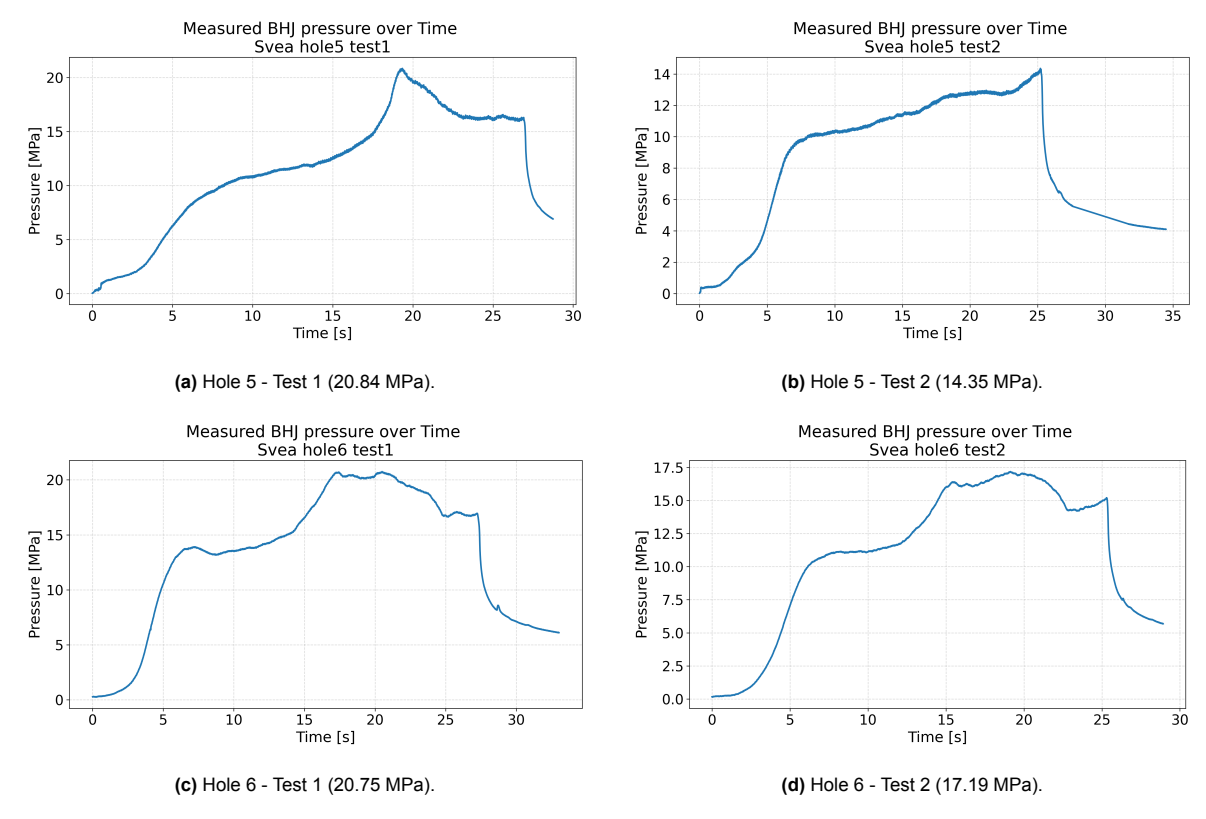


Figure A.7: Pressure vs Time plots for Hole 5 and Hole 6 at Svea.

A.2. Svea 60

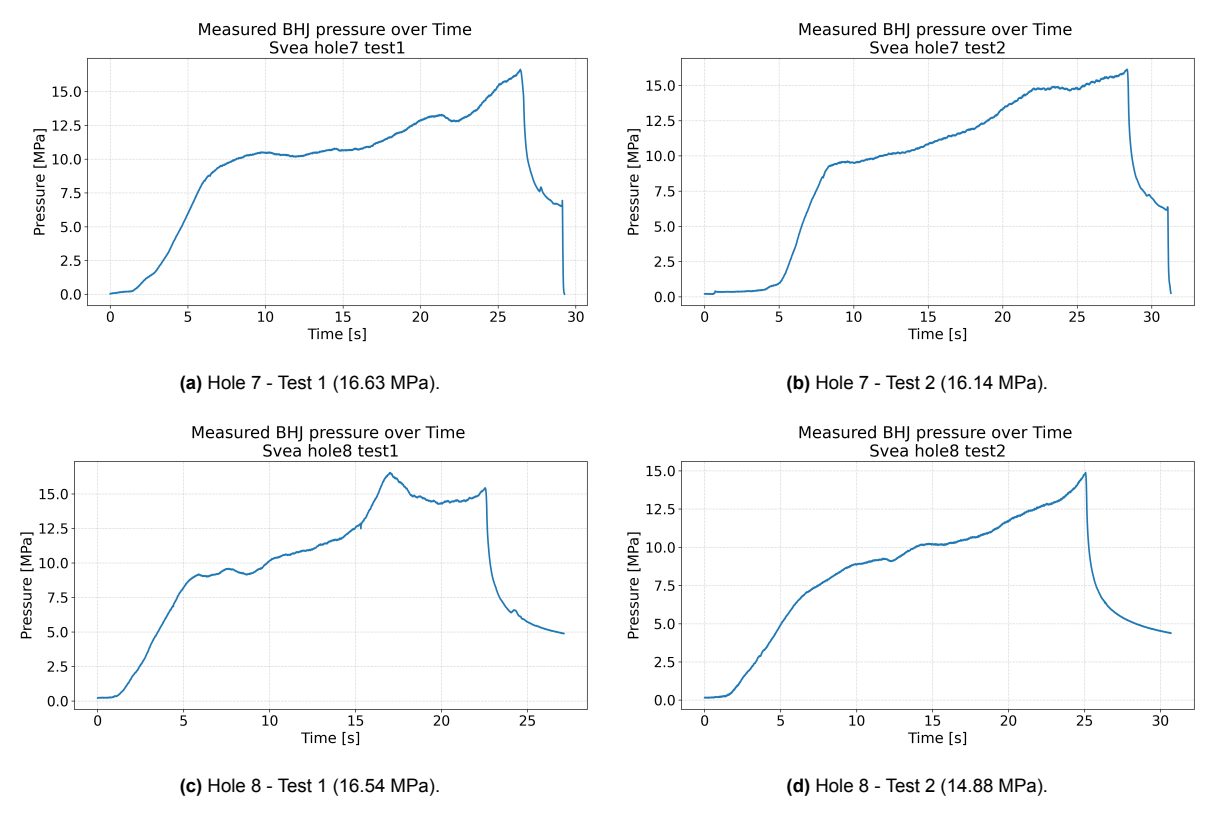


Figure A.8: Pressure vs Time plots for Hole 7 and Hole 8 at Svea.

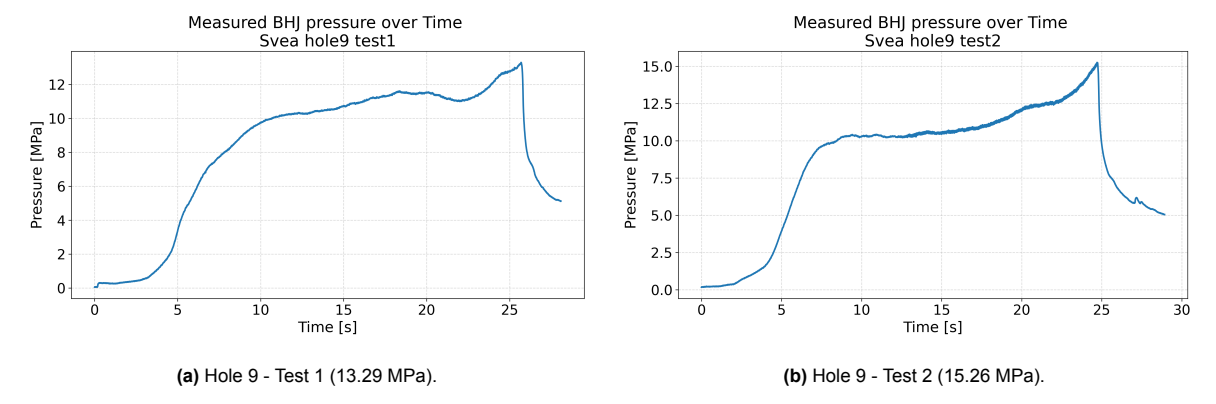


Figure A.9: Pressure vs Time plots for Hole 9 at Svea.